Open access • Posted Content • DOI:10.1101/2021.08.30.458303

Altered interaction between RBD and ACE2 receptor contributes towards the increased transmissibility of SARS CoV-2 delta, kappa, beta, and gamma strains with RBD double mutations. — Source link

Siddharth Sinha, Benjamin Tam, San Ming Wang

Institutions: University of Macau

Published on: 31 Aug 2021 - bioRxiv (Cold Spring Harbor Laboratory)

Topics: Host cell membrane

Altered interaction between RBD and ACE2 receptor contributes towards the increased transmissibility of SARS CoV-2 delta, kappa, beta, and gamma strains with RBD double mutations

Siddharth Sinha*, Benjamin Tam*, San Ming Wang#

Frontiers Science Center for Precision Oncology,
Faculty of Health Sciences, University of Macau, Macau

*Contributed equally to the study.

#Correspondence:
San Ming Wang, MD
Faculty of Health Sciences
University of Macau
Macau, SAR
China
Tel. +853 88224836
Fax. +853 88222314
Email: sanmingwang@um.edu.mo

ABSTRACT

The COVID-19 pandemics by SARS-CoV-2 causes catastrophic damage for global human health. The initial step of SARS-CoV-2 infection is the binding of the receptor-binding domain (RBD) in its spike protein to ACE2 receptor in host cell membrane. The evolving of SARS-CoV-2 constantly generates new mutations across its genome including RBD. Besides the well-known single mutation in RBD, the recent new mutation strains with RBD "double mutation" is causing new outbreaks globally, as represented by the delta strain containing RBD L452R/T478K. Although it is considered that the increased transmissibility of the double mutated strains could be attributed to the alteration of mutated RBD to ACE2 receptor, the molecular details remains to be unclear. Using the methods of molecular dynamics simulation, superimposed structural comparison, free binding energy estimation and antibody escaping, we investigated the relationship between ACE2 receptor and the RBD double mutant L452R/T478K (delta), L452R/E484Q (kappa) and E484K/N501Y (beta, gamma). The results demonstrated that each of the three RBD double mutants altered RBD structure, led to enhanced binding affinity of mutated RBD to ACE2 receptor, leading to increased transmissibility of SARS-CoV-2 to the host cells.

Keywords: SARS_CoV-2, Variants, MD simulations, Free energy, Antibody escape.

INTRODUCTION

SARS-CoV-2 pandemic has caused devastating consequences on global public health, with over 207 million people infected and over 4.3 million loss of life globally since the COVID-19 started (https://covid19.who.int accessed August 17, 2021). SARS-CoV-2 infects human cells through its spike (S) protein. In the process, the receptor-binding domain (RBD, residues 318–526) of the S protein (residues 1-1273)binds to the angiotensin-converting enzyme 2 (ACE2) receptor on host cell membrane to release its genome into the cell (Lan et al., 2020; Q. Wang et al., 2020). Therefore, RBD is a determinant for SARS-CoV-2 infection into host cells. As RNA virus, the genome of SARS-CoV-2 is constantly evolving with new mutations generated across its genome including RBD. Since the first SARS-CoV-2 genome sequences reported in Jan 5, 2020, there have been 942 coding-changing mutations identified within the 193 positions of RBD, more than one mutation per day (942 mutations in 932 days), and 4.9 mutations per position on average (Supplementary table 1, http://cov-glue.cvr.gla.ac.uk/#/replacement, access July 31, 2021). While most of the mutations do not show pathogenic significance, the strains containing several RBD mutations, namely L452R (epsilon), T478K, E484K, E484Q, and N501Y, were selected (Figure 1) and have caused multiple outbreaks much due to the increased transmissibility of SARS-CoV-2 contributed by these RBD mutations (Leung et al., 2021), https://www.who.int/en/activities/tracking-SARS-CoV-2-variants/). Recently, several new SARS-CoV-2 strains with RBD “double mutations” are causing new challenge. The double mutations basically contain the same single mutations above, but they are more transmissible than the strains with corresponding single mutation. For example, the “delta” strain with RBD mutation L452R/T478K rapidly spreads to over 130 countries since it was identified in late 2020 (Torjesen, 2021), https://www.cdc.gov/mmwr/volumes/70/wr/mm7031e2). L452R/E484Q (kalpa) and E484K/N501Y (beta, gamma). Thus, understanding the mechanism of increased transmissibility in RBD double mutations is urgently needed to develop strategies to control their spreading. While studies revealed how RBD single mutations increased SARS-CoV-2 transmissibility, it remains to know whether the SARS-CoV-2 with RBD double mutations adopted the same or similar manners as the SARS-CoV-2 with RBD single mutations or gains new features considering the more aggressive behavior of SARS-CoV-2 with RBD double mutations than SARS-CoV-2 with single RBD mutations.

In this study, we investigated the relationship between ACE2 receptor and three major RBD double mutant L452R/T478K (delta), L452R/E484Q (kappa) and E484K/N501Y (beta, gamma). We used multiple methods to address the topic including molecular dynamics simulation (MDS), superimposed structural comparison, free binding energy estimation and antibody escaping. Molecular dynamics simulation measures conformational change of protein across a time period and uses the trajectories to describe the thermodynamics changes in RBD mutant structure (Karplus, 2002; Sinha & Wang, 2020), superimposed structural comparison allows direct visualization of the altered RBD structure by

the double mutated residues (Kufareva & Abagyan, 2012), free binding energy change estimates the affinity

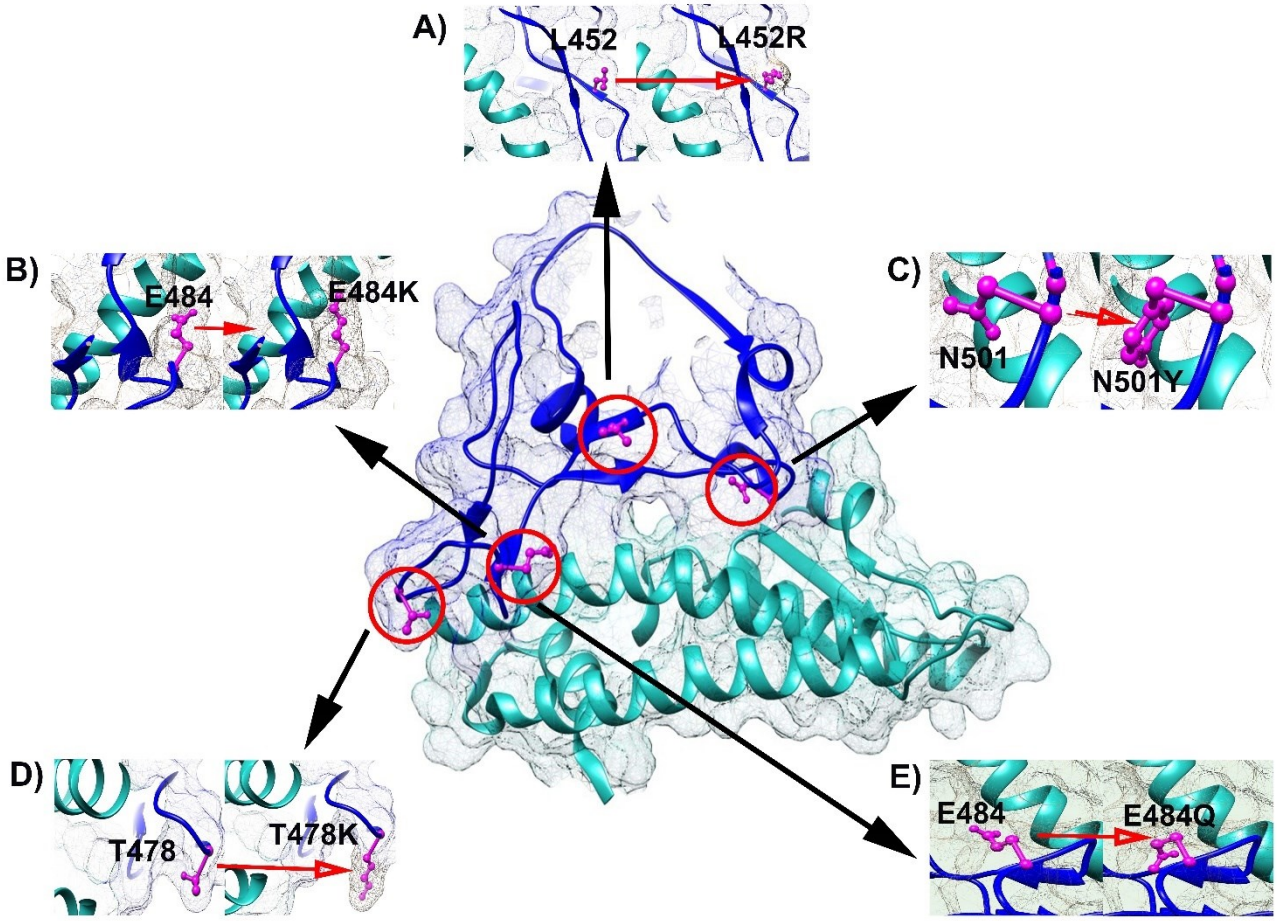

Figure 1. Locations of single mutated RBD and ACE2. The center shows the RBD-ACE2 complex, the surrounding shows the single mutations in RBD, with the left being the wild type and the right being the mutated residue. A) L452 and L452R; B) E484 and E484K; C) N501 and N501Y; D) T478 and T478K; E) E484 and E484Q.

change caused by the double mutated residues between RBD and ACE2 receptor (Gumbart et al., 2013), and mapping antibody binding site explains whether RBD structural change caused by mutated residues can result in escape of mutants from neutralizing antibodies (NAbs). The results from our study provided evidence that the three RBD double mutants altered RBD structure in the ways much different from these caused by the corresponding RBD single mutants, enhanced binding of mutated RBD to ACE2 receptor, leading to the high transmissibility of SARS-CoV-2 to the host cells.

RESULTS

Conformation changes in RBD double mutants

To investigate the effects of double mutations on RBD structure, we examined conformational changes of the RBD double mutant - ACE2 receptor complex in RBD double mutant L452R/T478K, L452R/E484Q, E484K/N501Y using MD simulations for 100 ns. We performed the study by using 5

different types of methods including simulations of RMSD (Root mean square deviation), RMSF (Root mean square fluctuation), Rg (radius of gyration), SASA (solvent accessible surface area) and MSD (mean square displacement) for each type of RBD double mutant, with the wild type RBD and 5 RBD single mutants as the controls. The results revealed substantial structural differences between the double mutants, wild type, and single mutants:

RMSD: It demonstrates the change in the atomic coordinates between the wildtype and mutant structures (Dong et al., 2018). The wild type RBD-ACE2 structure stabilized around ~0.3-0.4 nm with a deviation around 45 ns. L452R/T478K showed deviation upto ~30 ns and thereafter stabilized at ~0.3-0.4 nm**;** L452R/E484Q stabilized ~0.3-0.5 nm with a deviation at around 35 ns; E484K/N501Y reached equilibrium distance at ~0.23 nm. Single mutant L452R, T478K, E484Q and E484K all but N501Y showed stable configuration post 60 ns: L452R stabilized ~0.25 nm, T478K ~0.3 nm, E484Q ~0.2 – 0.3 nm, E484K ~0.3 nm. N501Y had 0.5 nm between 80 -100 ns. The results showed the trajectories in each of the RBD double mutants differed from the wild type and the corresponding single mutants (Figure 2).

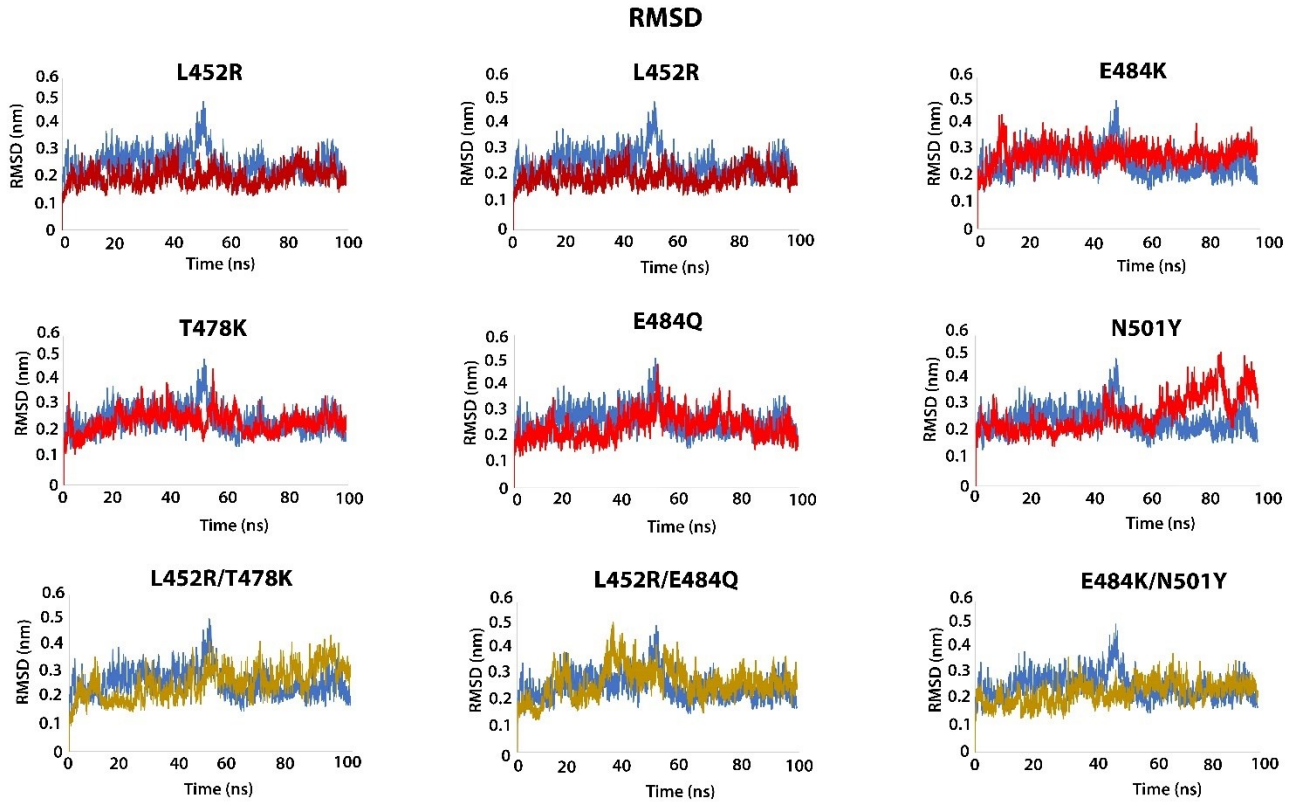

Figure 2. Dynamic changes of RBD structure by RMSD analysis. Blue: Wildtype, Red: single mutations (L452R, T478K, E484K, E484Y, N501Y); Yellow: double mutations (L452R/T478K, L452R/E484Q, E484K/N501Y). x-axis shows the simulation lasted time (100 ns), y-axis shows the RMSD value for the structures. The results show substantial differences between single and double mutated RBD structure.

RMSF: It determines the resilience of residues to analyze the effects of substitution in native and mutant structures (Benson & Daggett, 2012). The flexibility in polypeptide chain through RMSF showed that double mutant L452R/E484Q, L452R/T478K, and E484K/N501Y had high to medium resilience ~ 0.4 nm, ~0.15 nm, and ~0.25 nm, respectively, at residue position 360-380 and 470-490. In comparison, the single mutants had no greater flexibility in the backbone C-α atom than the native structure (Supplementary Figure 1). The higher resilience in the double mutant L452R/E484Q and E484K/N501Y can be attributed to their differences in RMSD trajectory around residue position 360-380 and 470-490.

Rg: It measures the compactness between the wild type and mutant structures (Daidone et al., 2003). Rg value for the wild type RBD was ~3.10-3.15 nm. Double mutant L452R/T478K showed a greater Rg value ~3.2-3.25 nm for the entire trajectory than the wild type**;** L452R/E484Q had ~3.13-3.18 nm; E484K/N501Y had ~3.15-3.25 nm after 35 ns; L452R/E484Q and E484K/N501Y showed the change in Rg value ~80-100 ns and ~10-30 ns respectively. Their larger hydrodynamic radius implies the change in the shape of structure during protein folding and unfolding. T478K, E484K, and E484Q had higher Rg values than the wild type RBD but lower than the double mutants, except N501Y had higher value ~3.2-3.3 nm (Supplementary Figure 2).

SASA: SASA defines the solvent accessible surface area thereby measuring the relative expansion of the native and mutant structures (Zhang & Lazim, 2017). The wild type RBD had a surface area of ~430 nm^2, all single mutant L452R, T478K, E484K, E484Q and N501Y had decreased value of ~426 nm^2, ~426 nm^2, ~424 nm^2, ~428 nm^2 and ~429 nm^2, respectively. The double mutants also decreased values to these in single mutants but their patterns were different (Supplementary Figure 3).

MSD: MSD defines the mean square displacement of overall atoms from a set of initial positions between wild type RBD and RBD mutants (Yousefpour et al., 2015). The wild type structure showed an average displacement value ~11.31. The double mutant L452R/T478K, L452R/E484Q and E484K/N501Y showed average displacement value ~10.88, ~7.33 and ~9.06, respectively, lower than the wild type but higher than these in the single mutants (Supplementary Figure 4).

Conformational changes in RBD double mutants

To directly visualize the conformational changes in double mutated RBD, we superimposed structure between wildtype, double mutants and the corresponding single mutants. We observed that the conformational changes in each of the double mutant RBD were substantially different from these in their corresponding single mutants (Figure 3). L452R/T478K showed conformational change at residue position 475-482 and 518-521 (Figure 3G), whereas both L452R/E484Q and E484K/N501Y were at residue position 475-485 (Figure 3H, 3I). L452 at the middle and N501 at the end of RBD-

ACE2 interface of the β strand attributes to the change in conformations of related mutants. L452R induced conformational change at residue position 474-485 and 517-526 (Figure 3B), whereas N501Y at residue position 439-453 and 498-502 (Figure 3F). The conformational changes in double mutants comprising of L452R and N501Y were very different from their corresponding single mutants.

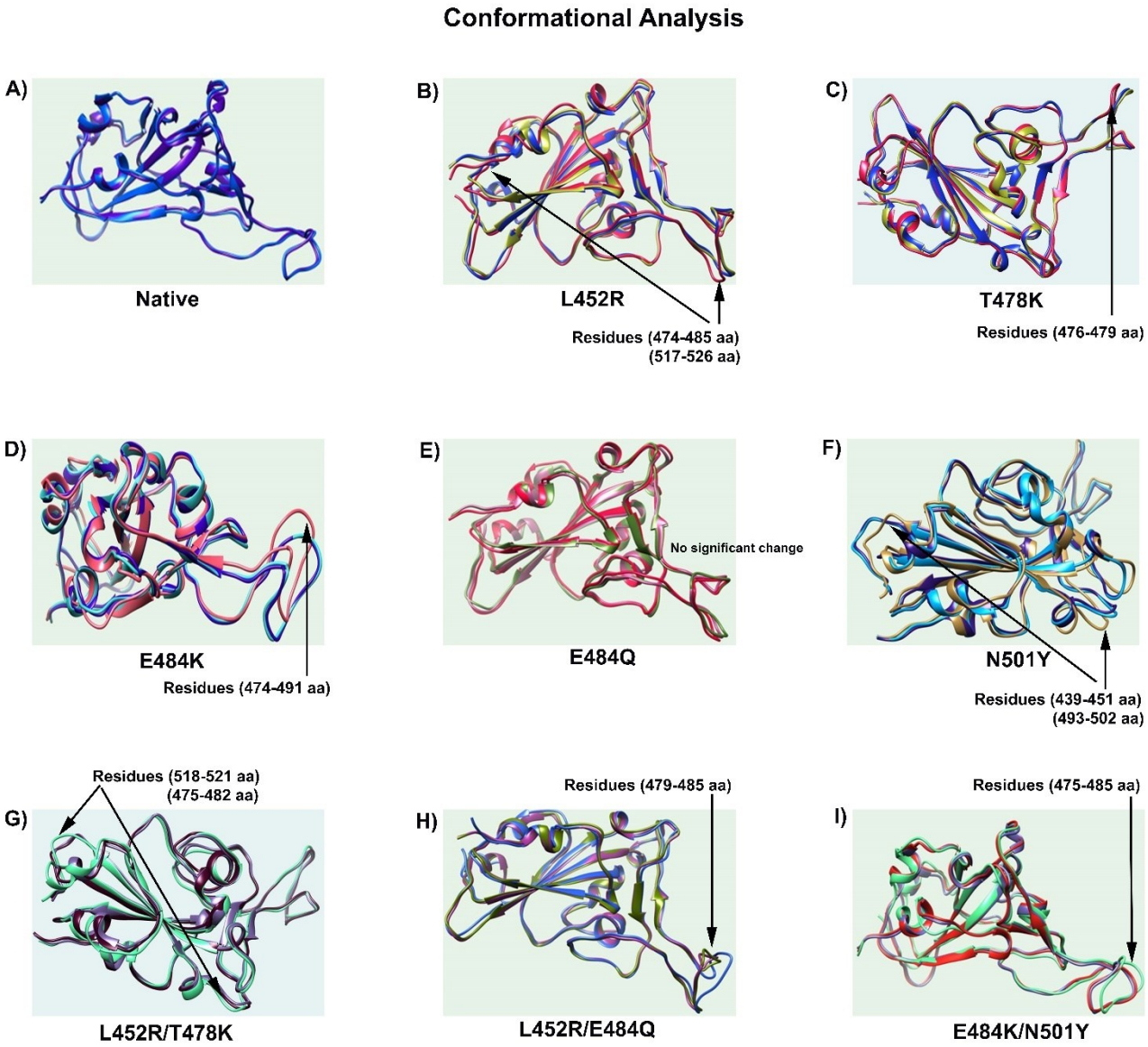

Figure 3. Conformational changes in mutated RBD. Mutant structures were superimposed with the wildtype RBD. Arrow shows conformation changes at specific residue positions. A) Native; B) L452R; C) T478K; D) E484K; E) E484Q; F) N501Y; G) L452R/T478K; H) L452R/E484Q; I) E484K/N501Y. The results show that the RBD conformational changes in double mutations were substantially different from single mutations.

Free energy changes in RBD double mutants

We used MM/GBSA method to estimate overall changes of free binding energy between RBD mutants and ACE2 receptor. The high binding energy of RBD to ACE2 receptor is largely contributed by several key residues including N501, L452 and T478, which had 4, 2 and 2 contact regions, respectively, whereas other residues such as E484 contributed less binding energy than N501 to ACE2 receptor (Figure 4). Comparing to the overall free binding energy of 212.5 kJ mol^{-1} between the wild type RBD and ACE2 receptor, all single and double RBD mutants showed increased free binding energy except N501Y decreased to -204.6 kJ mol^{-1} (Table 1A). However, the changed levels between double mutants and their corresponding single mutants were at similar levels, implying double mutants didn't generate higher binding energy than the single mutants.

We also compared the energy changes in the non-mutated residues in the RBD mutants. In the wild type RBD, a set of residues made high contributions to the overall energy between RBD and ACE2 receptor with the top 5 residues of F456, F486, Q493, T500, and Y505 (Table 1B). However, the top 5 residues in each RBD double mutant were mostly changed from the wild type RBD and their corresponding single mutations: L452/T478K changed to Y505, F486, N501, Q493, and T500; L452R/E484Q to F486, Q493, Y505, Y489 and F456; and E484K/N501Y to Y501, Y505, Q493, T500 and F486. N501 in the wildtype RBD contributed only -7.58 kJ mol^{-1} (9^{th}) in the 198 RBD residues (data not shown). However, N501 became a top residue in 2 of the 3 RBD double mutants and 4 of the 5 RBD single mutants, highlighting that N501Y in RBD double mutants and single RBD mutants played significant roles in enhancing the affinity between RBD mutants to ACE2 receptor by enhancing the binding energy (Table 1B, Figure 4).

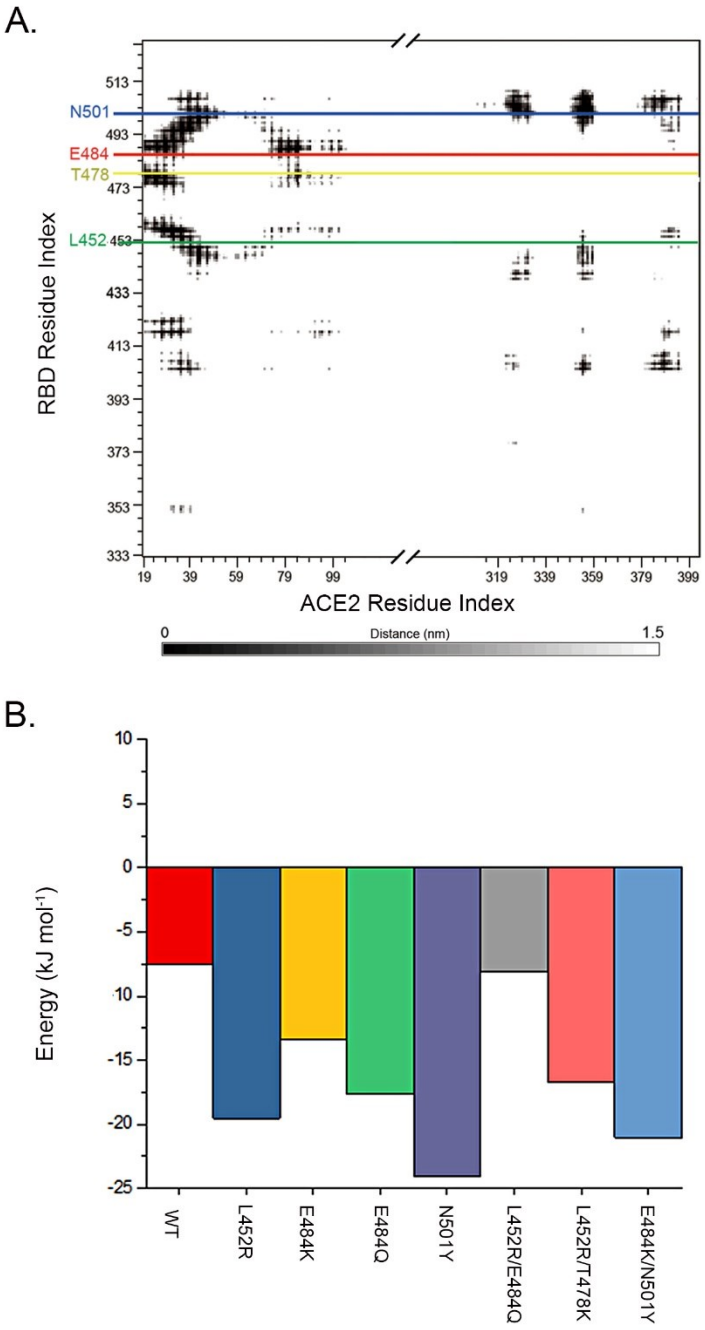

Figure 4. Free binding energy changes between mutated RBD and ACE2 receptor. A. RBD and ACE2 residue interaction map. Residues in close contact and the contact distance further than 1.5 nm are represented by diminishing grey scale. The key mutation positions (L452, T478, E484, N501) in RBD are highlighted in green, yellow, red and blue; B) binding energy by MM/GBSA for single RBD residues at position 501. It shows that while N501Y caused the highest increase of the binding energy at position 501, all single mutation (L452R, E484K, E484Q) and double mutation (L452R/E484Q, L452R/T478K, E484K/N501Y) also increased the binding energy at position 501. The red, blue, gold, green, purple, gray, pink and light blue represented WT, L452R, E484K, E484Q, N501Y, L452R/E484Q, L452R/T478K and E484K/N501Y, respectively.

Table 1. Free binding energy changes between mutated RBD and ACE2

Mutant	Residue	Free binding energy (kJ mol^{-1})
A, Overall free binding energy changes		
Wild type		-212.5
L452R		-288.1
T478K		-229.6
E484Q		-250.2
E484K		-243.0
N501Y		-204.6
L452R/T478K		-256.1
L452R/E484Q		-252.6
E484K/N501Y		-264.5
B. Top 5 non-mutated residues with free binding energy changes		
Wild type	Q493	-19.50
	Y505	-19.12
	F486	-14.85
	T500	-12.55
	F456	-11.41
L452R	Q498	-23.58
	Q493	-19.57
	N501	-19.54
	Y505	-18.89
	F486	-16.23
T478K	Y505	-19.15
	F486	-15.92
	Q493	-14.16
	T500	-13.62
	F456	-11.63
E484K	Y505	-21.61
	F486	-15.50
	T500	-13.73
	N501	-13.36
	Y489	-12.77
E484Q	Q493	-18.24
	N501	-17.64
	Y505	-17.16
	F486	-15.14
	F456	-12.33
N501Y	Y501	-24.05
	F486	-15.66
	Y505	-14.54
	F456	-12.23
	Q493	-11.86
L452R/T478K	Y505	-19.47
	F486	-17.49
	N501	-16.69
	Q493	-13.63
	T500	-12.99
L452R/E484Q	F486	-16.43
	Q493	-15.38
	Y505	-14.36
	Y489	-13.17
	F456	-12.56
E484K/N501Y	Y501	-21.05
	Y505	-16.95
	Q493	-16.35
	T500	-15.79
	F486	-14.90

Antibody escaping in RBD double mutants

SARS-CoV-2 neutralizing antibody (NAb) C121 (PDB ID: 7K8Z) is a well-known neutralizing antibody to SARS-CoV-2 through binging to RBD and E484K is a well-known mutant resistant to C121 binding (Barnes et al., 2020; Weisblum et al., 2020). We used C121 antibody and E484K as the model to test the relationship between RBD double mutants and antibody resistance. Figure 5 showed that the binding sites of C121 on S protein covering N439, N440, L455, G446, E484 and Q493 shown in yellow and E484K shown in green. Comparison of the binding sites between wild type RBD and double mutant RBD demonstrated that all three RBD double mutants altered C121 binding site, with L452R/E484Q as the most significant one among the three RBD double mutants. The results highlight L452R/E484K not only increased transmission but also facilitated antibody escape ability on SARS-CoV-2.

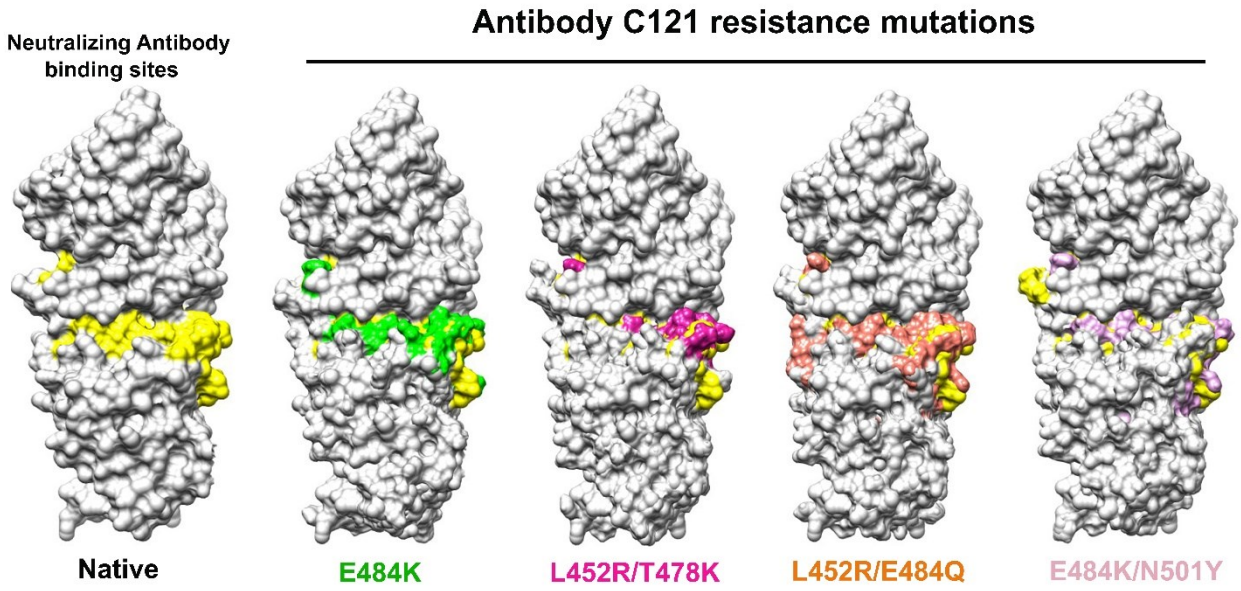

Figure 5. Changes of antibody binding sites in double mutated RBD. The binding site (N439, N440, L455, G446, E484 and Q493) of neutralizing antibody C121 (PDB ID: 7K8X) are compared between the wild type, E484K known escaping C121 binding, and double mutants L452R/T478K, L452R/E484Q and E484K/N501Y. Yellow: C121 binding sites on wild type RBD; Green: C121 binding sites on E484K RBD; Magenta: C121 binding sites on L452R/T478K RBD; Orange: C121 binding sites on L452R/E484Q RBD; Pink: C121 binding sites on E484K/N501Y RBD. The figure shows that all three double mutated RBD altered the C121 biding sites, with L452R/T478K (delta) as the most significant one.

DISCUSSION

It has been proposed that higher transmissibility of SARS-CoV-2 new mutant strains can be attributed by the increased affinity of the mutated RBD to ACE2 receptor in the host cells, and the RBD double mutations can further increase the affinity and enhance the transmissibility, as represented by SARS-CoV-2 L452R/T478K (delta), L452R/E484Q (kappa), E484K/N501Y (beta and gamma) strains (Scudellari, 2021). Using combinational methods, our study provides structural-based evidence to demonstrate that RBD double mutant-changed RBD structure enhances the affinity of mutated RBD to ACE2 receptor, causing the increased transmissibility of the new SARS-CoV-2 mutant strains.

It is interesting to note that many of the "hot spot" mutants predicted by previous simulation studies have rarely become highly transmissible strains (Gan et al., 2021; Ghorbani et al., 2020; Y. Wang et al., 2020; Yi et al., 2020). Instead, only limited numbers of mostly unpredicted single mutations were truly selected to cause outbreaks. More interesting fact is that the RBD double mutations in the newly emerging strains still inherited these mutations at the same positions with different combinations. This indicates that although MDS is powerful in detecting structural changes caused by mutation, solely based on physical relationship between RBD and ACE2 receptor in the randomly detected mutation pool is not a reliable approach to determine the "hotspot" mutation as the marks for new strain with increased transmissibility. No matter how strong the physical interaction between mutated RBD to ACE2 receptor, only these with best fitness within the mutation pool will be selected, which is determined by multiple selection factors not only by the relationship between RBD and ACE2 receptor. In addition, relying on the accumulated quantity of mutation sequences may also give misleading information for the increased transmissibility, as the number of sequences collected could be biased sampling, not necessarily reflect the actual abundance of the mutant strains in actual infected population. This is reflected by the RBD mutation sequence data that only 4 (N501Y, L452R, E484K, Y478K) were listed among the 7 top mutation sequences, and E484Q was listed at 26th position (Supplementary table 1). Therefore, focusing on the "real world" mutations either single, double and possible triple combinations at these fixed positions can provide more reliable evidence to monitor the newly selected strains and to use the physical evidence to explain the structural basis for these highly selected ones with high transmissibility (Khan et al., 2021).

N501 is particularly interesting residue. It has been determined that N501 enhances RBD binding to ACE2 by maintaining RBD at open conformation (Teruel *et al*., 2021), and this function can be enhanced by E484K (Nelson *et al*, 2021). N501 is also a mutation hot-spot as reflected by the RBD single mutation N501Y in the alpha strain (Fiorentini et al., 2021), and RBD double mutation E484K/N501Y in beta and gamma strains. We observed that each tested RBD single or double mutation increased the free binding energy between N501 and ACE2 receptor (Figure 4B), highlighting that N501 is a key player in enhancing wile type and mutated RBD binding to ACE2, not

only for N501Y but also the mutated residues in other RBD locations likely through allosteric activity (Mugnai et al., 2020). For example, E484K and E484Q substantially increased binding affinity of N501 and N501Y to ACE2 receptor (Luan et al., 2021; Nelson et al., 2021). Similar situation was also present in RBD double mutants, and mutations outside RBD can also contribute to the increased affinity of RBD to ACE2 receptor, such as D614G (Korber et al., 2020).Therefore, not only the mutated RBD residues but also non-mutated RBD residues needs to be considered when addressing the increased transmissibility of new mutant strains.

Antibody resistance is one of the crucial determinants of viral transmission. Many potentially neutralizing anti SARS-CoV-2 antibodies target RBD to block its binding to the ACE-2 receptor (Baum et al., 2020; Ju et al., 2020; Starr et al., 2021). Consistent with experimental observations (Rogers et al., 2020), our study showed that all three RBD double mutants can cause antibody escape. Breakthrough infection by delta strain has been observed in the vaccinated individuals (Bergwerk et al., 2021). Our observation indicates that the altered antibody binding sites on RBD by RBD double mutation contributes to the phenomenon.

It is interesting to note that the binding energy between single mutants (L452R, T478K, E484K, E484Q and N501Y) and double mutants (L452/E484Q, L452/T478K and E484K/N501Y) were at similar level, although both were higher than the wild type RBD.

In conclusion, our study revealed that double mutated RBD in SARS-CoV-2 caused the changes of RBD structure, RBD binding energy to ACE2 receptor, and antibody binding sites on RBD. These changes contribute to the increased transmissibility of recent SARS-CoV-2 mutant strains with double mutated RBD.

MATERIALS & METHODS

Structures of RBD and mutated RBDs

The structure of SARS-CoV-2 RBD - ACE2 receptor complex (PDB ID: 6M0J) was used as the wild type reference (Lan et al., 2020). The structure was optimized using CHARMM36m force field in GROMACS version 5.1.2. Three RBD double mutant L452R/T478K (delta), L452R/E484Q (Kappa) and E484K/N501Y (beta, gamma), and 5 RBD single mutants of L452R, T478K, E484Q, E484K, and N501Y included in the double mutants were used in the study. The structures with the mutated residues in each mutant were generated using UCSF Chimera following the default parameters (Pettersen et al., 2004).

Molecular dynamics simulation

GROMACS version 5.1.2, was used for molecular dynamics simulation (Berendsen et al., 1995). CHARMM36m force field was chosen to model RBD - ACE2 receptor complex (Huang et al., 2017). The complex was situated in the simulation box 2 nm away from the box edge. The system was solvated with tip3p water and neutralized with Na+ ions. Steep descent algorithm was applied to the system before 1 ns equilibration run at 298 K and 1 bar in the NPT ensemble using Berendsen thermostat and barostat. The system was set at 298 K and 1 bar in the NPT ensemble by using a V-rescale thermostat and Parrinello-Rahman barostat during the production run (Parrinello & Rahman, 1981). Verlet velocity algorithm was employed with a time step of 2 fs. The Particle Mesh Ewald (PME) method was used to treat the long-range electrostatic interactions with the cut-off distance at 1.0 nm. Hydrogen bond was constrained at equilibrium lengths by the LINC algorithm and the trajectory frame of MD was saved every 30 ps (Hess, 2008). RMSD, RMSF, Rg, SASA and MSD were used to analyze structural changes of the native RBD and its mutants. The 35-40ns simulation trajectories were utilized in each method. XMGRACE program was utilized to generate the corresponding plots (Turner, 2005). Three independent RMSD MD simulations were performed for the wild type RBD-ACE2 for 100 ns, received RBD values at 0.186 nm, 0.173 nm, 0.179 nm, ACE2 values at 0.229 nm, 0.230 nm, 0.239 nm for run 1, run 2, run 3. The results confirmed that RBD - ACE2 structure remained stable throughout the simulation process.

Superimposed structural comparison

Mutant RBD structures extracted at 100 ns of MD simulations through UCSF CHIMERA were superimposed with the wild type RBD structures to identify the conformation changes using PYMOL.

Antibody escaping analysis

To determine whether RBD mutants escape the binding by neutralization antibody, structures between the mutant and wildtype RBD were structurally mapped with independent binding sites of antibody C121 on RBD. The RBD binding site for antibody C121, a neutralizing antibody known to bind RBD (PDB: 7K8X) (Barnes et al., 2020; Weisblum et al., 2020), and E484K mutant known to escape C121 binding were used to determine the impact of double mutant L452R/T478K, L452R/E484Q and E484K/N501Y on antibody binding structure.

Free binding energy calculation

MM/GBSA **(**molecular mechanics energies combined with generalized Born and surface area continuum solvation) (Genheden & Ryde, 2015) was used to calculate the free binding energy of the RBD to ACE2 (http://cadd.zju.edu.cn/hawkdock,(Weng et al., 2019). ff02 force field (Cieplak et al., 2001) and the GB^{OBC1} model (Onufriev et al., 2004) were assigned upon the proteins (Complex, RBD

and ACE2) before steepest descent and conjugate gradient minimization. The free energy of binding, ΔG, is calculated based on the following equation:

$$\Delta G = G(complex) - G(RBD) - G(ACE2)$$

For each component, the total energy was estimated by using the following equation:

$$G = G_{bond} + G_{elec} + G_{vdW} + G_{pol} + G_{np} - TS$$

The first three terms represent the standard MM energy terms: bonded (bond, angle, and dihedral), electrostatic and van der Waal interactions. G_{pol} and G_{np} are the polar and the non-polar contribution of solvation free energies, calculated by the Generalised Born (GB) implicit solvent method and solvent accessible surface area (SASA). The last term absolute temperature, T, is multiplied by entropy, S. For the double mutant RBD and their containing single mutant RBD, simulation was performed at 100 ns and a single protein coordinate file was extracted every 10 ns. Overall free binding energy was averaged for each type of RBD.

Acknowledgements

We are thankful for the Information and Communication Technology Office (ICTO), University of Macau for providing the High-Performance Computing Cluster (HPCC) resource and facilities for the study.

Contribution

SS, BT: method development, analysis, data acquisition and interpretation, draft manuscript; SMW: conception, design, data analysis and interpretation, draft and revise manuscript, and funding.

Funding

This work was supported by Macau Science and Technology Development Fund (085/2017/A2, 0077/2019/AMJ), University of Macau (SRG2017-00097-FHS, MYRG2019-00018-FHS), Faculty of Health Sciences, University of Macau (FHSIG/SW/0007/2020P, Startup fund) (SMW).

Competing interests

None declared.

Patient consent for publication

Not required.

Ethics approval

Not required.

Data availability

All data relevant to the study are included in the article or uploaded as online supplemental information.

REFERENCES

Lan, J., Ge, J., Yu, J., Shan, S., Zhou, H., Fan, S., Zhang, Q., Shi, X., Wang, Q., Zhang, L., & Wang, X. (2020). Structure of the SARS-CoV-2 spike receptor-binding domain bound to the ACE2 receptor. Nature, 581(7807), 215-220. https://doi.org/10.1038/s41586-020-2180-5

Wang, Q., Zhang, Y., Wu, L., Niu, S., Song, C., Zhang, Z., Lu, G., Qiao, C., Hu, Y., Yuen, K. Y., Wang, Q., Zhou, H., Yan, J., & Qi, J. (2020). Structural and Functional Basis of SARS-CoV-2 Entry by Using Human ACE2. *Cell*, *181*(4), 894-904.e899. https://doi.org/10.1016/j.cell.2020.03.045

Leung, K., Shum, M. H., Leung, G. M., Lam, T. T., & Wu, J. T. (2021). Early transmissibility assessment of the N501Y mutant strains of SARS-CoV-2 in the United Kingdom, October to November 2020. *Euro Surveillance*, *26*(1). https://doi.org/10.2807/1560-7917.Es.2020.26.1.2002106

Torjesen, I. (2021). Covid-19: Delta variant is now UK's most dominant strain and spreading through schools. *BMJ*, *373*, n1445. https://doi.org/10.1136/bmj.n1445

Karplus, M. (2002). Molecular Dynamics Simulations of Biomolecules. *Accounts of Chemical Research*, *35*(6), 321-323. https://doi.org/10.1021/ar020082r

Sinha, S., & Wang, S. M. (2020). Classification of VUS and unclassified variants in BRCA1 BRCT repeats by molecular dynamics simulation. *Computational and Structural Biotechnology Journal*, *18*, 723-736. https://doi.org/10.1016/j.csbj.2020.03.013

Kufareva, I., & Abagyan, R. (2012). Methods of protein structure comparison. *Methods in Molecular Biology*, *857*, 231-257. https://doi.org/10.1007/978-1-61779-588-6_10

Gumbart, J. C., Roux, B., & Chipot, C. (2013). Efficient Determination of Protein–Protein Standard Binding Free Energies from First Principles. *Journal of Chemical Theory and Computation*, *9*(8), 3789-3798. https://doi.org/10.1021/ct400273t

Dong, Y. W., Liao, M. L., Meng, X. L., & Somero, G. N. (2018). Structural flexibility and protein adaptation to temperature: Molecular dynamics analysis of malate dehydrogenases of marine molluscs. *Proceedings of the National Academy of Sciences*, *115*(6), 1274-1279. https://doi.org/10.1073/pnas.1718910115

Benson, N. C., & Daggett, V. (2012). A Comparison of Multiscale Methods for the Analysis of Molecular Dynamics Simulations. *The Journal of Physical Chemistry B*, *116*(29), 8722-8731. https://doi.org/10.1021/jp302103t

Daidone, I., Amadei, A., Roccatano, D., & Nola, A. D. (2003). Molecular Dynamics Simulation of Protein Folding by Essential Dynamics Sampling: Folding Landscape of Horse Heart Cytochrome c. *Biophysical Journal*, *85*(5), 2865-2871. https://doi.org/https://doi.org/10.1016/S0006-3495(03)74709-2

Zhang, D., & Lazim, R. (2017). Application of conventional molecular dynamics simulation in evaluating the stability of apomyoglobin in urea solution. *Scientific Reports*, *7*, 44651. https://doi.org/10.1038/srep44651

Yousefpour, A., Modarress, H., Goharpey, F., & Amjad-Iranagh, S. (2015). Interaction of PEGylated anti-hypertensive drugs, amlodipine, atenolol and lisinopril with lipid bilayer membrane: A molecular dynamics simulation study. *Biochim Biophys Acta*, *1848*(8), 1687-1698. https://doi.org/10.1016/j.bbamem.2015.04.016

Barnes, C. O., Jette, C. A., Abernathy, M. E., Dam, K. A., Esswein, S. R., Gristick, H. B., Malyutin, A. G., Sharaf, N. G., Huey-Tubman, K. E., Lee, Y. E., Robbiani, D. F., Nussenzweig, M. C., West, A. P., Jr., & Bjorkman, P. J. (2020). SARS-CoV-2 neutralizing antibody structures inform therapeutic strategies. *Nature*, *588*(7839), 682-687. https://doi.org/10.1038/s41586-020-2852-1

Weisblum, Y., Schmidt, F., Zhang, F., DaSilva, J., Poston, D., Lorenzi, J. C., Muecksch, F., Rutkowska, M., Hoffmann, H. H., Michailidis, E., Gaebler, C., Agudelo, M., Cho, A., Wang, Z., Gazumyan, A., Cipolla, M., Luchsinger, L., Hillyer, C. D., Caskey, M., Robbiani, D. F., Rice, C. M., Nussenzweig, M. C., Hatziioannou, T., & Bieniasz, P. D. (2020). Escape from neutralizing antibodies by SARS-CoV-2 spike protein variants. *Elife*, *9*, e61312. https://doi.org/10.7554/eLife.61312

Scudellari, M. (2021). How the coronavirus infects cells - and why Delta is so dangerous. *Nature*, *595*(7869), 640-644. https://doi.org/10.1038/d41586-021-02039-y

Gan, H. H., Twaddle, A., Marchand, B., & Gunsalus, K. C. (2021). Structural Modeling of the SARS-CoV-2 Spike/Human ACE2 Complex Interface can Identify High-Affinity Variants Associated with Increased Transmissibility. *J Mol Biol*, *433*(15), 167051. https://doi.org/10.1016/j.jmb.2021.167051

Ghorbani, M., Brooks, B. R., & Klauda, J. B. (2020). Critical Sequence Hotspots for Binding of Novel Coronavirus to Angiotensin Converter Enzyme as Evaluated by Molecular Simulations. *The Journal of Physical Chemistry B*, *124*(45), 10034-10047. https://doi.org/10.1021/acs.jpcb.0c05994

Wang, Y., Liu, M., & Gao, J. (2020). Enhanced receptor binding of SARS-CoV-2 through networks of hydrogen-bonding and hydrophobic interactions. *Proceedings of the National Academy of Sciences*, *117*(25), 13967-13974. https://doi.org/10.1073/pnas.2008209117

Yi, C., Sun, X., Ye, J., Ding, L., Liu, M., Yang, Z., Lu, X., Zhang, Y., Ma, L., Gu, W., Qu, A., Xu, J., Shi, Z., Ling, Z., & Sun, B. (2020). Key residues of the receptor binding motif in the spike protein of SARS-CoV-2 that interact with ACE2 and neutralizing antibodies. *Cellular & Molecular Immunology*, *17*(6), 621-630. https://doi.org/10.1038/s41423-020-0458-z

Khan, A., Zia, T., Suleman, M., Khan, T., Ali, S. S., Abbasi, A. A., Mohammad, A., & Wei, D. Q. (2021). Higher infectivity of the SARS-CoV-2 new variants is associated with K417N/T, E484K, and N501Y mutants: An insight from structural data. *Journal of Cellular Physiology*. https://doi.org/10.1002/jcp.30367

Teruel N, Mailhot O, Najmanovich RJ (2021) Modelling conformational state dynamics and its role on infection for SARS-CoV-2 Spike protein variants. PLoS Comput Biol 17(8): e1009286. https://doi.org/10.1371/journal.pcbi.1009286

Fiorentini, S., Messali, S., Zani, A., Caccuri, F., Giovanetti, M., Ciccozzi, M., & Caruso, A. (2021). First detection of SARS-CoV-2 spike protein N501 mutation in Italy in August, 2020. *The Lancet Infectious Diseases*, *21*(6), e147. https://doi.org/10.1016/S1473-3099(21)00007-4

Mugnai, M. L., Templeton, C., Elber, R., & Thirumalai, D. (2020). Role of Long-range Allosteric Communication in Determining the Stability and Disassembly of SARS-COV-2 in Complex with ACE2. *bioRxiv*. https://doi.org/10.1101/2020.11.30.405340

Luan, B., Wang, H., & Huynh, T. (2021). Molecular Mechanism of the N501Y Mutation for Enhanced Binding between SARS-CoV-2's Spike Protein and Human ACE2 Receptor. *bioRxiv*, 2021.2001.2004.425316. https://doi.org/10.1101/2021.01.04.425316

Nelson, G., Buzko, O., Spilman, P., Niazi, K., Rabizadeh, S., & Soon-Shiong, P. (2021). Molecular dynamic simulation reveals E484K mutation enhances spike RBD-ACE2 affinity and the combination of E484K, K417N and N501Y mutations (501Y.V2 variant) induces conformational change greater than N501Y mutant alone, potentially resulting in an escape mutant. *bioRxiv*, 2021.2001.2013.426558. https://doi.org/10.1101/2021.01.13.426558

Korber, B., Fischer, W. M., Gnanakaran, S., Yoon, H., Theiler, J., Abfalterer, W., Hengartner, N., Giorgi, E. E., Bhattacharya, T., Foley, B., Hastie, K. M., Parker, M. D., Partridge, D. G., Evans, C. M., Freeman, T. M., de Silva, T. I., Angyal, A., Brown, R. L., Carrilero, L., Green, L. R., Groves, D. C., Johnson, K. J., Keeley, A. J.,

Lindsey, B. B., Parsons, P. J., Raza, M., Rowland-Jones, S., Smith, N., Tucker, R. M., Wang, D., Wyles, M. D., McDanal, C., Perez, L. G., Tang, H., Moon-Walker, A., Whelan, S. P., LaBranche, C. C., Saphire, E. O., & Montefiori, D. C. (2020). Tracking Changes in SARS-CoV-2 Spike: Evidence that D614G Increases Infectivity of the COVID-19 Virus. *Cell*, *182*(4), 812-827.e819. https://doi.org/https://doi.org/10.1016/j.cell.2020.06.043

Baum, A., Fulton, B. O., Wloga, E., Copin, R., Pascal, K. E., Russo, V., Giordano, S., Lanza, K., Negron, N., Ni, M., Wei, Y., Atwal, G. S., Murphy, A. J., Stahl, N., Yancopoulos, G. D., & Kyratsous, C. A. (2020). Antibody cocktail to SARS-CoV-2 spike protein prevents rapid mutational escape seen with individual antibodies. *Science*, *369*(6506), 1014-1018. https://doi.org/10.1126/science.abd0831

Ju, B., Zhang, Q., Ge, J., Wang, R., Sun, J., Ge, X., Yu, J., Shan, S., Zhou, B., Song, S., Tang, X., Yu, J., Lan, J., Yuan, J., Wang, H., Zhao, J., Zhang, S., Wang, Y., Shi, X., Liu, L., Zhao, J., Wang, X., Zhang, Z., & Zhang, L. (2020). Human neutralizing antibodies elicited by SARS-CoV-2 infection. *Nature*, *584*(7819), 115-119. https://doi.org/10.1038/s41586-020-2380-z

Starr, T. N., Czudnochowski, N., Liu, Z., Zatta, F., Park, Y. J., Addetia, A., Pinto, D., Beltramello, M., Hernandez, P., Greaney, A. J., Marzi, R., Glass, W. G., Zhang, I., Dingens, A. S., Bowen, J. E., Tortorici, M. A., Walls, A. C., Wojcechowskyj, J. A., De Marco, A., Rosen, L. E., Zhou, J., Montiel-Ruiz, M., Kaiser, H., Dillen, J., Tucker, H., Bassi, J., Silacci-Fregni, C., Housley, M. P., di Iulio, J., Lombardo, G., Agostini, M., Sprugasci, N., Culap, K., Jaconi, S., Meury, M., Dellota, E., Abdelnabi, R., Foo, S. C., Cameroni, E., Stumpf, S., Croll, T. I., Nix, J. C., Havenar-Daughton, C., Piccoli, L., Benigni, F., Neyts, J., Telenti, A., Lempp, F. A., Pizzuto, M. S., Chodera, J. D., Hebner, C. M., Virgin, H. W., Whelan, S. P. J., Veesler, D., Corti, D., Bloom, J. D., & Snell, G. (2021). SARS-CoV-2 RBD antibodies that maximize breadth and resistance to escape. *Nature*. https://doi.org/10.1038/s41586-021-03807-6

Rogers, T. F., Zhao, F., Huang, D., Beutler, N., Burns, A., He, W. T., Limbo, O., Smith, C., Song, G., Woehl, J., Yang, L., Abbott, R. K., Callaghan, S., Garcia, E., Hurtado, J., Parren, M., Peng, L., Ramirez, S., Ricketts, J., Ricciardi, M. J., Rawlings, S. A., Wu, N. C., Yuan, M., Smith, D. M., Nemazee, D., Teijaro, J. R., Voss, J. E., Wilson, I. A., Andrabi, R., Briney, B., Landais, E., Sok, D., Jardine, J. G., & Burton, D. R. (2020). Isolation of potent SARS-CoV-2 neutralizing antibodies and protection from disease in a small animal model. *Science (New York, N.Y.)*, *369*(6506), 956-963. https://doi.org/10.1126/science.abc7520

Bergwerk, M., Gonen, T., Lustig, Y., Amit, S., Lipsitch, M., Cohen, C., Mandelboim, M., Gal Levin, E., Rubin, C., Indenbaum, V., Tal, I., Zavitan, M., Zuckerman, N., Bar-Chaim, A., Kreiss, Y., & Regev-Yochay, G. (2021). Covid-19 Breakthrough Infections in Vaccinated Health Care Workers. *New England Journal of Medicine*. https://doi.org/10.1056/NEJMoa2109072

Pettersen, E. F., Goddard, T. D., Huang, C. C., Couch, G. S., Greenblatt, D. M., Meng, E. C., & Ferrin, T. E. (2004). UCSF Chimera—A visualization system for exploratory research and analysis. *Journal of Computational Chemistry*, *25*(13), 1605-1612. https://doi.org/10.1002/jcc.20084

Berendsen, H. J. C., van der Spoel, D., & van Drunen, R. (1995). GROMACS: A message-passing parallel molecular dynamics implementation. *Computer Physics Communications*, *91*(1), 43-56. https://doi.org/https://doi.org/10.1016/0010-4655(95)00042-E

Hess, B. (2008). P-LINCS: A Parallel Linear Constraint Solver for Molecular Simulation. *Journal of Chemical Theory and Computation*, *4*(1), 116-122. https://doi.org/10.1021/ct700200b

Parrinello, M., & Rahman, A. (1981). Polymorphic transitions in single crystals: A new molecular dynamics method. *Journal of Applied Physics*, *52*(12), 7182-7190. https://doi.org/10.1063/1.328693

Turner, P. (2005). XMGRACE, Version 5.1. 19. *Center for Coastal and Land-Margin Research, Oregon Graduate Institute of Science and Technology, Beaverton, OR*.

Barnes, C. O., Jette, C. A., Abernathy, M. E., Dam, K. A., Esswein, S. R., Gristick, H. B., Malyutin, A. G., Sharaf, N. G., Huey-Tubman, K. E., Lee, Y. E., Robbiani, D. F., Nussenzweig, M. C., West, A. P., Jr., & Bjorkman, P. J. (2020). SARS-CoV-2 neutralizing antibody structures inform therapeutic strategies. *Nature*, *588*(7839), 682-687. https://doi.org/10.1038/s41586-020-2852-1

Genheden, S., & Ryde, U. (2015). The MM/PBSA and MM/GBSA methods to estimate ligand-binding affinities. *Expert opinion on drug discovery*, *10*(5), 449-461. https://doi.org/10.1517/17460441.2015.1032936

Cieplak, P., Caldwell, J., & Kollman, P. (2001). Molecular mechanical models for organic and biological systems going beyond the atom centered two body additive approximation: aqueous solution free energies of methanol and N-methyl acetamide, nucleic acid base, and amide hydrogen bonding and chloroform/water partition coefficients of the nucleic acid bases. *Journal of Computational Chemistry*, *22*(10), 1048-1057. https://doi.org/https://doi.org/10.1002/jcc.1065

Onufriev, A., Bashford, D., & Case, D. A. (2004). Exploring protein native states and large-scale conformational changes with a modified generalized born model. *Proteins*, *55*(2), 383-394. https://doi.org/10.1002/prot.20033

Additional Supplementary Files

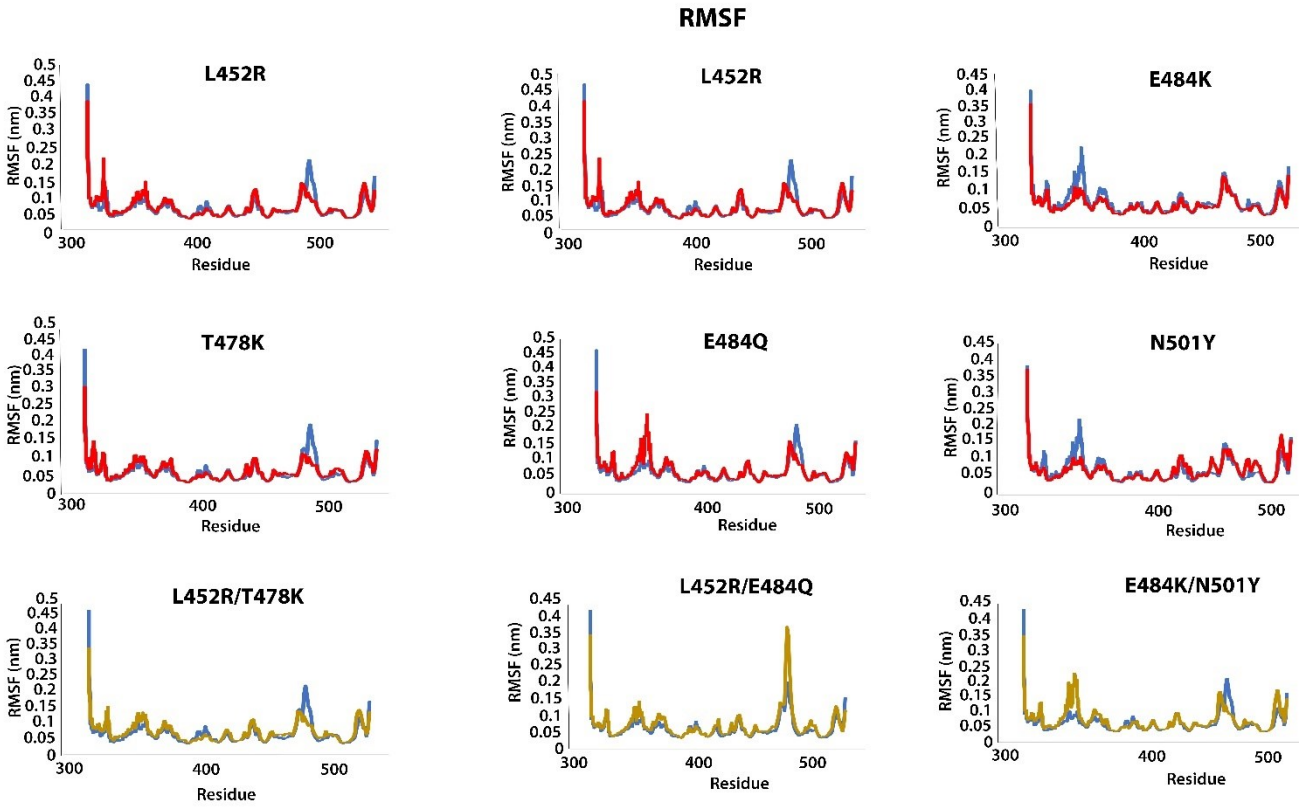

S. Figure 1. Dynamic changes of RBD structure by RMSF analysis in wildtype, single and double mutant structures. The x-axis represents the residue positions of the RBD domain and y-axis represents the RMSF value for the structures. Blue: wild type; red: single mutant; yellow: double mutants.

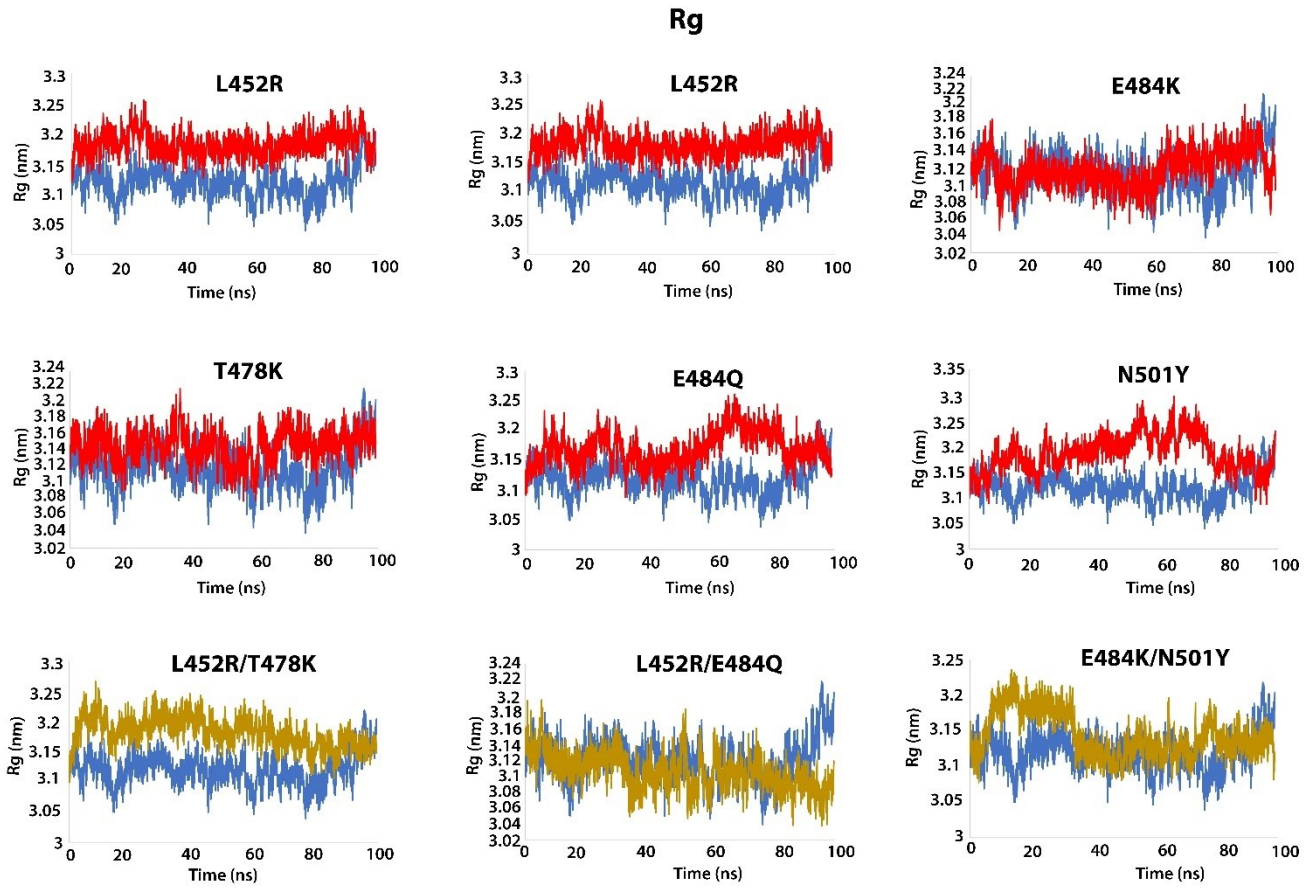

S. Figure 2. Dynamic changes of RBD structure by Rg analysis in in wildtype, single and double mutant structures. The x-axis represents the time period of 100 ns and y-axis represents the Rg value for the structures. Blue: wild type; red: single mutant; yellow: double mutants.

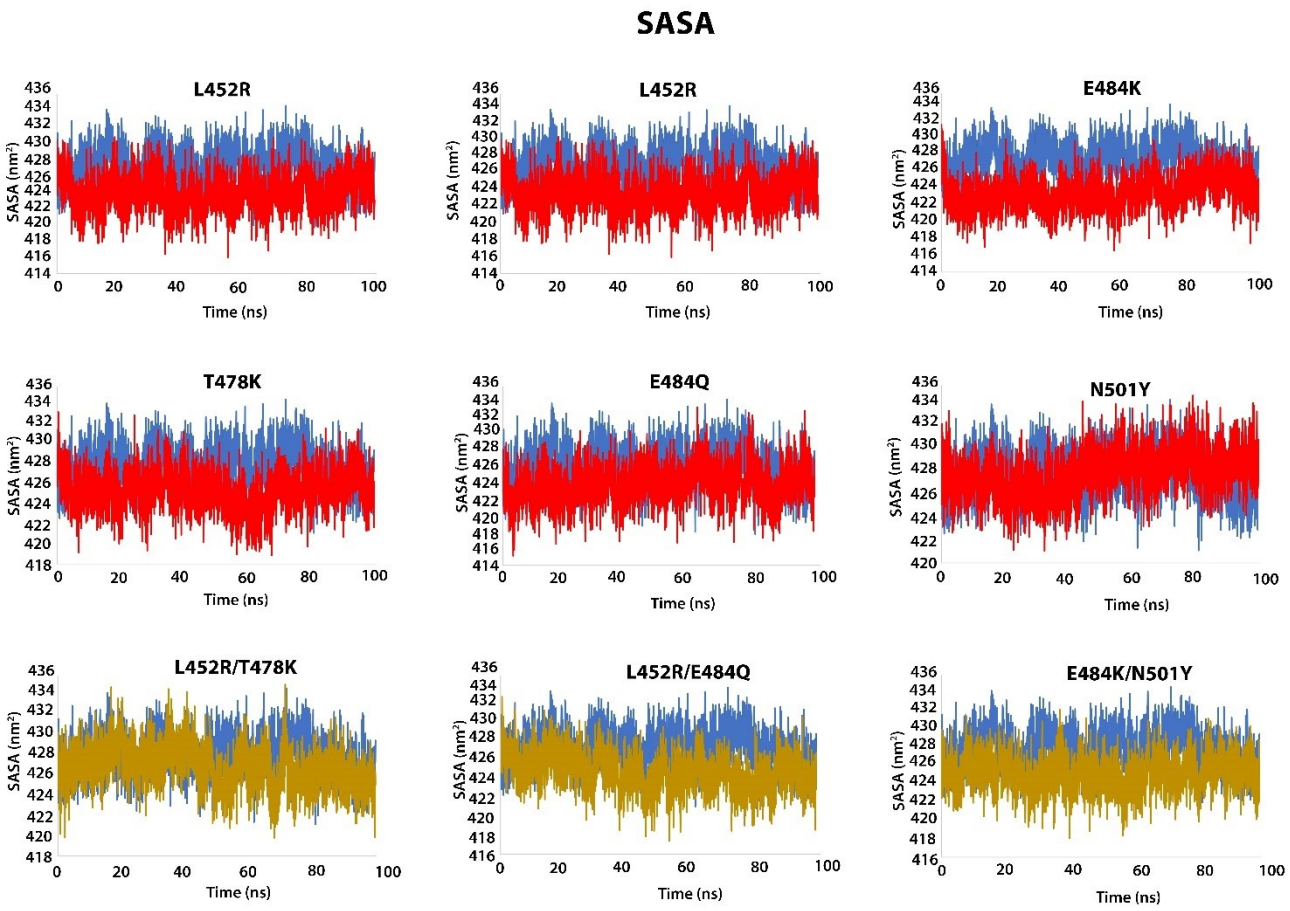

S. Figure 3. Dynamic changes of RBD structure by SASA analysis in wildtype, single and double mutant structures. The x-axis represents the time period of 100 ns and y-axis represents the SASA value for the structures. Blue: wild type; red: single mutant; yellow: double mutants.

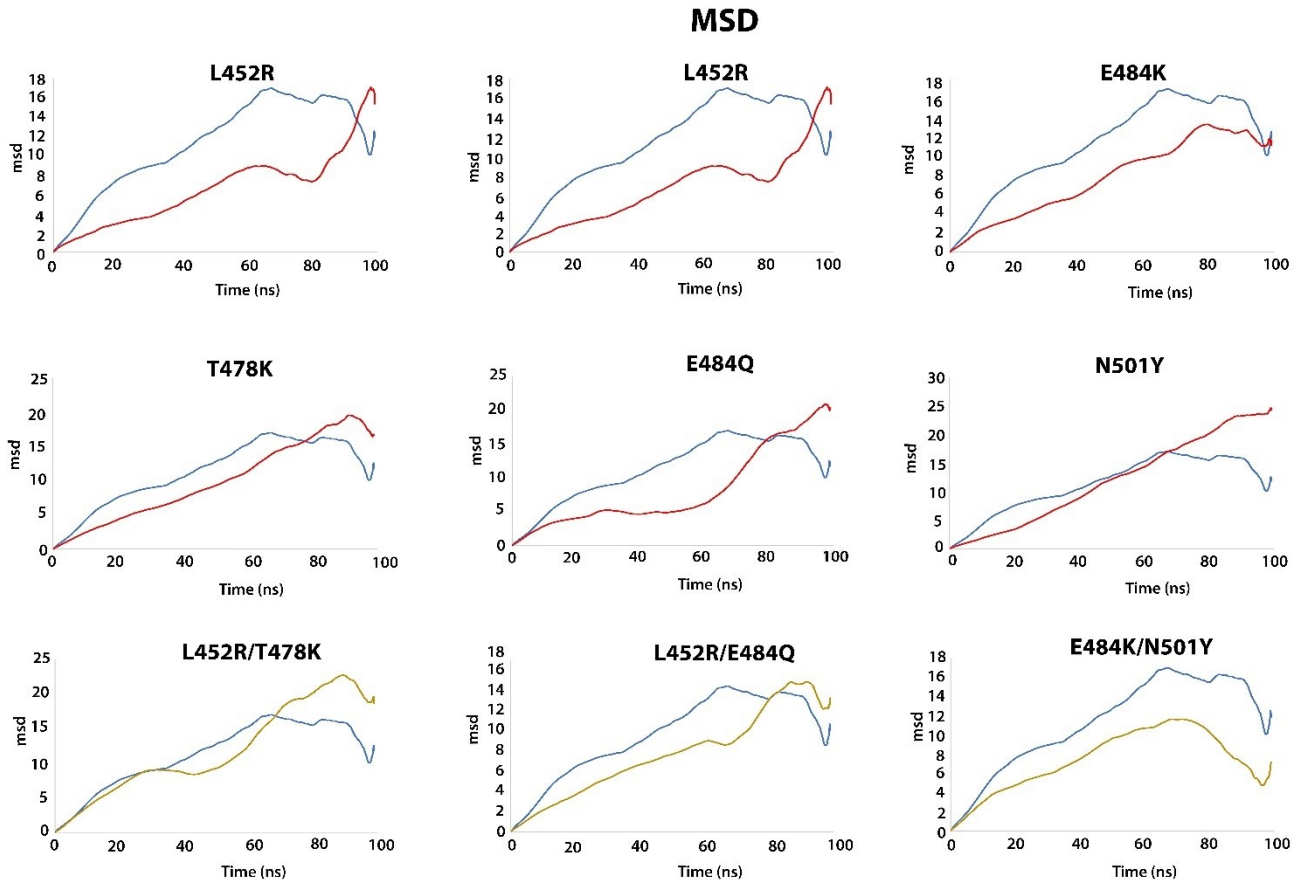

S. Figure 4. Dynamic changes of RBD structure by MSD analysis in wildtype, single and double mutant structures. The x-axis represents the time period of 100 ns and y-axis represents the MSD value for the structures. Blue: wild type; red: single mutant; yellow: double mutants.

Supplementary table 1. RBD missense mutations identified (http://cov-glue.cvr.gla.ac.uk/#/replacement, access July 31, 2021)

Replacement	Codon Number	Ref Nt Position	Ref. Amino Acid	Replaced Amino Acid	Num seqs
N501Y	501	23063	N	Y	257333
S477N	477	22991	S	N	36814
L452R	452	22916	L	R	22334
N439K	439	22877	N	K	21141
E484K	484	23012	E	K	16426
K417N	417	22811	K	N	6595
T478K	478	22994	T	K	6559
S494P	494	23042	S	P	2862
N501T	501	23063	N	T	2167
K417T	417	22811	K	T	1616
V367F	367	22661	V	F	1100
Y453F	453	22919	Y	F	981
N440K	440	22880	N	K	929
P384L	384	22712	P	L	896
S477R	477	22991	S	R	754
F490S	490	23030	F	S	612
G446V	446	22898	G	V	603
T323I	323	22529	T	I	585
P330S	330	22550	P	S	542
V382L	382	22706	V	L	493
R357K	357	22631	R	K	472
P384S	384	22712	P	S	379
R346K	346	22598	R	K	364
P479S	479	22997	P	S	361
S477I	477	22991	S	I	346
E484Q	484	23012	E	Q	300
T478I	478	22994	T	I	298
S459F	459	22937	S	F	292
T385I	385	22715	T	I	291
L452Q	452	22916	L	Q	268
Q414K	414	22802	Q	K	255
Q414R	414	22802	Q	R	232

L455F	455	22925	L	F	222
A348S	348	22604	A	S	219
K444*	444	22892	K	*	208
Y508H	508	23084	Y	H	207
A475V	475	22985	A	V	203
T478R	478	22994	T	R	202
V483F	483	23009	V	F	195
N448Y	448	22904	N	Y	191
A344S	344	22592	A	S	189
N354D	354	22622	N	D	183
L452M	452	22916	L	M	174
N450K	450	22910	N	K	170
S373L	373	22679	S	L	169
F318L	318	22514	F	L	167
Q321E	321	22523	Q	E	167
A352S	352	22616	A	S	164
V320G	320	22520	V	G	148
G476S	476	22988	G	S	147
R408K	408	22784	R	K	142
F490L	490	23030	F	L	136
N481K	481	23003	N	K	134
T376I	376	22688	T	I	128
N354K	354	22622	N	K	127
E406Q	406	22778	E	Q	122
T385N	385	22715	T	N	116
S359N	359	22637	S	N	106
R403K	403	22769	R	K	105
K356R	356	22628	K	R	104
R408I	408	22784	R	I	104
I410V	410	22790	I	V	104
N370S	370	22670	N	S	103
F338L	338	22574	F	L	102
V483A	483	23009	V	A	100
V367L	367	22661	V	L	94

A411S	411	22793	A	S	90
A475S	475	22985	A	S	90
E471Q	471	22973	E	Q	89
V327I	327	22541	V	I	84
L335F	335	22565	L	F	84
G339D	339	22577	G	D	84
D427N	427	22841	D	N	82
K444N	444	22892	K	N	76
V362F	362	22646	V	F	75
T470I	470	22970	T	I	74
K444R	444	22892	K	R	73
G496S	496	23048	G	S	73
V341I	341	22583	V	I	69
S373P	373	22679	S	P	69
V367I	367	22661	V	I	68
P322S	322	22526	P	S	66
S459Y	459	22937	S	Y	64
A372V	372	22676	A	V	63
I434V	434	22862	I	V	63
I468V	468	22964	I	V	63
V320I	320	22520	V	I	62
S494L	494	23042	S	L	61
G446S	446	22898	G	S	59
V503I	503	23069	V	I	59
G404C	404	22772	G	C	58
G485V	485	23015	G	V	58
G339S	339	22577	G	S	57
A419S	419	22817	A	S	57
A348T	348	22604	A	T	54
T470N	470	22970	T	N	54
K458N	458	22934	K	N	53
P463S	463	22949	P	S	52
S373A	373	22679	S	A	50
Y508C	508	23084	Y	C	50

N394Y	394	22742	N	Y	48
I402V	402	22766	I	V	48
P412L	412	22796	P	L	47
R346S	346	22598	R	S	46
Q493K	493	23039	Q	K	46
K378N	378	22694	K	N	45
P330L	330	22550	P	L	44
Q493L	493	23039	Q	L	44
F486L	486	23018	F	L	43
V503F	503	23069	V	F	43
E324V	324	22532	E	V	42
G485R	485	23015	G	R	42
N370H	370	22670	N	H	41
T415N	415	22805	T	N	41
S477G	477	22991	S	G	41
P479L	479	22997	P	L	41
Q493R	493	23039	Q	R	41
E324Q	324	22532	E	Q	40
A352V	352	22616	A	V	40
F318S	318	22514	F	S	39
R346I	346	22598	R	I	39
N370K	370	22670	N	K	39
T430I	430	22850	T	I	38
V445A	445	22895	V	A	38
E484G	484	23012	E	G	38
Q321L	321	22523	Q	L	36
D427Y	427	22841	D	Y	36
E471D	471	22973	E	D	36
A348V	348	22604	A	V	35
N354S	354	22622	N	S	35
P384R	384	22712	P	R	34
L390F	390	22730	L	F	34
N448H	448	22904	N	H	33
V320F	320	22520	V	F	32

L368I	368	22664	L	I	30
V401L	401	22763	V	L	30
V407I	407	22781	V	I	30
I468T	468	22964	I	T	30
E484A	484	23012	E	A	30
P499S	499	23057	P	S	30
T415A	415	22805	T	A	29
G476A	476	22988	G	A	29
F490Y	490	23030	F	Y	29
Y505H	505	23075	Y	H	29
N331T	331	22553	N	T	28
D405Y	405	22775	D	Y	28
N501S	501	23063	N	S	28
N354H	354	22622	N	H	27
V367A	367	22661	V	A	27
D427G	427	22841	D	G	27
Y449H	449	22907	Y	H	27
Q321K	321	22523	Q	K	26
V433F	433	22859	V	F	26
Q493H	493	23039	Q	H	26
G482S	482	23006	G	S	25
P337S	337	22571	P	S	24
R346G	346	22598	R	G	24
E471K	471	22973	E	K	24
I472V	472	22976	I	V	24
V483I	483	23009	V	I	24
Q321*	321	22523	Q	*	23
S349P	349	22607	S	P	23
G485S	485	23015	G	S	23
Q506K	506	23078	Q	K	23
T323A	323	22529	T	A	22
A435S	435	22865	A	S	22
L441F	441	22883	L	F	22
E471G	471	22973	E	G	22

G485A	485	23015	G	A	22
G413W	413	22799	G	W	21
Q414*	414	22802	Q	*	21
N440Y	440	22880	N	Y	21
N448S	448	22904	N	S	21
G504S	504	23072	G	S	21
E340D	340	22580	E	D	20
N440T	440	22880	N	T	20
Y451H	451	22913	Y	H	20
A475T	475	22985	A	T	20
N394T	394	22742	N	T	19
V445I	445	22895	V	I	19
G447V	447	22901	G	V	19
T470A	470	22970	T	A	19
I472T	472	22976	I	T	19
N481D	481	23003	N	D	19
P499H	499	23057	P	H	19
N501I	501	23063	N	I	19
P507S	507	23081	P	S	19
V320A	320	22520	V	A	18
T323R	323	22529	T	R	18
A344T	344	22592	A	T	18
F329L	329	22547	F	L	17
A344V	344	22592	A	V	17
S366P	366	22658	S	P	17
D427H	427	22841	D	H	17
D427V	427	22841	D	V	17
P479H	479	22997	P	H	17
P491L	491	23033	P	L	17
Y505W	505	23075	Y	W	17
E324D	324	22532	E	D	16
S325F	325	22535	S	F	16
P337T	337	22571	P	T	16
T393I	393	22739	T	I	16

V445F	445	22895	V	F	16
F456L	456	22928	F	L	16
K462N	462	22946	K	N	16
T470K	470	22970	T	K	16
G504D	504	23072	G	D	16
G339V	339	22577	G	V	15
E340K	340	22580	E	K	15
D389E	389	22727	D	E	15
L441I	441	22883	L	I	15
N460I	460	22940	N	I	15
S371P	371	22673	S	P	14
W436C	436	22868	W	C	14
G447S	447	22901	G	S	14
R457S	457	22931	R	S	14
E465D	465	22955	E	D	14
E484D	484	23012	E	D	14
F490V	490	23030	F	V	14
G496V	496	23048	G	V	14
E324K	324	22532	E	K	13
E340G	340	22580	E	G	13
W353C	353	22619	W	C	13
S375F	375	22685	S	F	13
N450D	450	22910	N	D	13
Y489H	489	23027	Y	H	13
P499L	499	23057	P	L	13
V503A	503	23069	V	A	13
P507L	507	23081	P	L	13
V320L	320	22520	V	L	12
T333I	333	22559	T	I	12
N334K	334	22562	N	K	12
C361*	361	22643	C	*	12
C361T	361	22643	C	T	12
F374L	374	22682	F	L	12
E406D	406	22778	E	D	12

G413R	413	22799	G	R	12
R466K	466	22958	R	K	12
N481S	481	23003	N	S	12
Q493*	493	23039	Q	*	12
T345S	345	22595	T	S	11
K356N	356	22628	K	N	11
Y369H	369	22667	Y	H	11
K378R	378	22694	K	R	11
D405E	405	22775	D	E	11
G413E	413	22799	G	E	11
T415I	415	22805	T	I	11
V433I	433	22859	V	I	11
P463L	463	22949	P	L	11
S469L	469	22967	S	L	11
V483L	483	23009	V	L	11
P491S	491	23033	P	S	11
Y495H	495	23045	Y	H	11
P507A	507	23081	P	A	11
V510L	510	23090	V	L	11
P322A	322	22526	P	A	10
C336S	336	22568	C	S	10
P337L	337	22571	P	L	10
E340A	340	22580	E	A	10
A352D	352	22616	A	D	10
I358V	358	22634	I	V	10
F377L	377	22691	F	L	10
D428G	428	22844	D	G	10
S438F	438	22874	S	F	10
S443A	443	22889	S	A	10
N460K	460	22940	N	K	10
L461I	461	22943	L	I	10
L461P	461	22943	L	P	10
G476C	476	22988	G	C	10
S494A	494	23042	S	A	10

S359G	359	22637	S	G	9
S359T	359	22637	S	T	9
S371F	371	22673	S	F	9
N394S	394	22742	N	S	9
S399L	399	22757	S	L	9
I402L	402	22766	I	L	9
A411T	411	22793	A	T	9
A411V	411	22793	A	V	9
G413V	413	22799	G	V	9
N440D	440	22880	N	D	9
N448D	448	22904	N	D	9
N448T	448	22904	N	T	9
I472L	472	22976	I	L	9
G476V	476	22988	G	V	9
S477T	477	22991	S	T	9
Q506*	506	23078	Q	*	9
I326V	326	22538	I	V	8
V327F	327	22541	V	F	8
P337H	337	22571	P	H	8
R357I	357	22631	R	I	8
S359R	359	22637	S	R	8
D364N	364	22652	D	N	8
S371T	371	22673	S	T	8
A372S	372	22676	A	S	8
A372T	372	22676	A	T	8
T376S	376	22688	T	S	8
G381R	381	22703	G	R	8
D389N	389	22727	D	N	8
V395I	395	22745	V	I	8
V395L	395	22745	V	L	8
R408T	408	22784	R	T	8
Q409*	409	22787	Q	*	8
K417R	417	22811	K	R	8
I418V	418	22814	I	V	8

P426S	426	22838	P	S	8
N440S	440	22880	N	S	8
G446A	446	22898	G	A	8
Y449S	449	22907	Y	S	8
E465G	465	22955	E	G	8
D467Y	467	22961	D	Y	8
Q474H	474	22982	Q	H	8
T500I	500	23060	T	I	8
T500S	500	23060	T	S	8
R328I	328	22544	R	I	7
P330A	330	22550	P	A	7
N334H	334	22562	N	H	7
S349F	349	22607	S	F	7
K356M	356	22628	K	M	7
K356T	356	22628	K	T	7
I358T	358	22634	I	T	7
V382A	382	22706	V	A	7
V407A	407	22781	V	A	7
I434L	434	22862	I	L	7
G446D	446	22898	G	D	7
C480R	480	23000	C	R	7
E484*	484	23012	E	*	7
P322L	322	22526	P	L	6
G339C	339	22577	G	C	6
A344F	344	22592	A	F	6
R346T	346	22598	R	T	6
W353L	353	22619	W	L	6
S375P	375	22685	S	P	6
Y380F	380	22700	Y	F	6
S383F	383	22709	S	F	6
V395F	395	22745	V	F	6
Y396H	396	22748	Y	H	6
A397S	397	22751	A	S	6
D398N	398	22754	D	N	6

D405G	405	22775	D	G	6
R408G	408	22784	R	G	6
P412Q	412	22796	P	Q	6
Q414L	414	22802	Q	L	6
G416*	416	22808	G	*	6
D428Y	428	22844	D	Y	6
W436L	436	22868	W	L	6
K444M	444	22892	K	M	6
G447D	447	22901	G	D	6
R457M	457	22931	R	M	6
S459P	459	22937	S	P	6
N460S	460	22940	N	S	6
N460T	460	22940	N	T	6
K462I	462	22946	K	I	6
K462T	462	22946	K	T	6
F464L	464	22952	F	L	6
F464S	464	22952	F	S	6
E471A	471	22973	E	A	6
Y473F	473	22979	Y	F	6
Q474*	474	22982	Q	*	6
Q474E	474	22982	Q	E	6
Q474R	474	22982	Q	R	6
G496R	496	23048	G	R	6
P499R	499	23057	P	R	6
T500A	500	23060	T	A	6
F318Y	318	22514	F	Y	5
P322T	322	22526	P	T	5
S325Y	325	22535	S	Y	5
N331S	331	22553	N	S	5
I332V	332	22556	I	V	5
F342L	342	22586	F	L	5
N343Y	343	22589	N	Y	5
V362L	362	22646	V	L	5
Y365D	365	22655	Y	D	5

A372P	372	22676	A	P	5
S375T	375	22685	S	T	5
T376N	376	22688	T	N	5
K378*	378	22694	K	*	5
C379F	379	22697	C	F	5
V382E	382	22706	V	E	5
T385P	385	22715	T	P	5
D389Y	389	22727	D	Y	5
L390I	390	22730	L	I	5
L390P	390	22730	L	P	5
Y396F	396	22748	Y	F	5
S399P	399	22757	S	P	5
R403S	403	22769	R	S	5
G404V	404	22772	G	V	5
I410T	410	22790	I	T	5
G416E	416	22808	G	E	5
D420N	420	22820	D	N	5
D420Y	420	22820	D	Y	5
G431V	431	22853	G	V	5
A435T	435	22865	A	T	5
G447C	447	22901	G	C	5
N450S	450	22910	N	S	5
Y453H	453	22919	Y	H	5
R457T	457	22931	R	T	5
K458E	458	22934	K	E	5
K458R	458	22934	K	R	5
E465*	465	22955	E	*	5
S469*	469	22967	S	*	5
T478A	478	22994	T	A	5
G482V	482	23006	G	V	5
E484R	484	23012	E	R	5
G485C	485	23015	G	C	5
N487D	487	23021	N	D	5
C488F	488	23024	C	F	5

C488R	488	23024	C	R	5
Y489*	489	23027	Y	*	5
Q498H	498	23054	Q	H	5
N501K	501	23063	N	K	5
P507Q	507	23081	P	Q	5
E324A	324	22532	E	A	4
S325A	325	22535	S	A	4
R328G	328	22544	R	G	4
R328S	328	22544	R	S	4
T333K	333	22559	T	K	4
F338S	338	22574	F	S	4
A344D	344	22592	A	D	4
T345F	345	22595	T	F	4
R346F	346	22598	R	F	4
F347L	347	22601	F	L	4
A348P	348	22604	A	P	4
W353R	353	22619	W	R	4
R355S	355	22625	R	S	4
N360S	360	22640	N	S	4
C361F	361	22643	C	F	4
C361S	361	22643	C	S	4
A363V	363	22649	A	V	4
D364Y	364	22652	D	Y	4
F374S	374	22682	F	S	4
F374Y	374	22682	F	Y	4
S375Y	375	22685	S	Y	4
K378M	378	22694	K	M	4
S383P	383	22709	S	P	4
N394I	394	22742	N	I	4
V395A	395	22745	V	A	4
R408S	408	22784	R	S	4
A411D	411	22793	A	D	4
G413A	413	22799	G	A	4
T415S	415	22805	T	S	4

A419T	419	22817	A	T	4
L425S	425	22835	L	S	4
P426L	426	22838	P	L	4
D427A	427	22841	D	A	4
T430A	430	22850	T	A	4
W436*	436	22868	W	*	4
N437S	437	22871	N	S	4
S438P	438	22874	S	P	4
D442Y	442	22886	D	Y	4
G446C	446	22898	G	C	4
Y449C	449	22907	Y	C	4
R454*	454	22922	R	*	4
L455S	455	22925	L	S	4
R457K	457	22931	R	K	4
K458Q	458	22934	K	Q	4
K462E	462	22946	K	E	4
K462R	462	22946	K	R	4
P463H	463	22949	P	H	4
I468F	468	22964	I	F	4
N481T	481	23003	N	T	4
G482A	482	23006	G	A	4
V483G	483	23009	V	G	4
E484V	484	23012	E	V	4
F486S	486	23018	F	S	4
N487Y	487	23021	N	Y	4
Y489C	489	23027	Y	C	4
Q498K	498	23054	Q	K	4
Q498R	498	23054	Q	R	4
P499T	499	23057	P	T	4
G502C	502	23066	G	C	4
R509I	509	23087	R	I	4
R509S	509	23087	R	S	4
R319I	319	22517	R	I	3
R319S	319	22517	R	S	3

R319T	319	22517	R	T	3
T323S	323	22529	T	S	3
R328K	328	22544	R	K	3
F329S	329	22547	F	S	3
C336Y	336	22568	C	Y	3
E340*	340	22580	E	*	3
T345A	345	22595	T	A	3
T345I	345	22595	T	I	3
S349A	349	22607	S	A	3
Y351H	351	22613	Y	H	3
R355T	355	22625	R	T	3
K356E	356	22628	K	E	3
I358L	358	22634	I	L	3
C361R	361	22643	C	R	3
A363P	363	22649	A	P	3
Y365H	365	22655	Y	H	3
Y365S	365	22655	Y	S	3
S366Y	366	22658	S	Y	3
S371A	371	22673	S	A	3
S373*	373	22679	S	*	3
C379S	379	22697	C	S	3
T385A	385	22715	T	A	3
K386R	386	22718	K	R	3
N388S	388	22724	N	S	3
C391*	391	22733	C	*	3
F392S	392	22736	F	S	3
T393A	393	22739	T	A	3
Y396C	396	22748	Y	C	3
Y396N	396	22748	Y	N	3
A397V	397	22751	A	V	3
S399*	399	22757	S	*	3
F400L	400	22760	F	L	3
R403G	403	22769	R	G	3
R403I	403	22769	R	I	3

G404S	404	22772	G	S	3
D405N	405	22775	D	N	3
E406*	406	22778	E	*	3
D420A	420	22820	D	A	3
D420G	420	22820	D	G	3
N422I	422	22826	N	I	3
L425F	425	22835	L	F	3
L425V	425	22835	L	V	3
P426Q	426	22838	P	Q	3
D428E	428	22844	D	E	3
T430S	430	22850	T	S	3
G431C	431	22853	G	C	3
I434M	434	22862	I	M	3
A435V	435	22865	A	V	3
D442V	442	22886	D	V	3
N448K	448	22904	N	K	3
Y451F	451	22913	Y	F	3
L452V	452	22916	L	V	3
Y453C	453	22919	Y	C	3
L455V	455	22925	L	V	3
K458*	458	22934	K	*	3
K458T	458	22934	K	T	3
L461F	461	22943	L	F	3
D467E	467	22961	D	E	3
D467V	467	22961	D	V	3
I468M	468	22964	I	M	3
S469A	469	22967	S	A	3
S469T	469	22967	S	T	3
E471*	471	22973	E	*	3
E471V	471	22973	E	V	3
Y473*	473	22979	Y	*	3
A475P	475	22985	A	P	3
G476D	476	22988	G	D	3
T478S	478	22994	T	S	3

C480*	480	23000	C	*	3
N481H	481	23003	N	H	3
N481I	481	23003	N	I	3
N481Y	481	23003	N	Y	3
G482C	482	23006	G	C	3
G482R	482	23006	G	R	3
N487I	487	23021	N	I	3
N487K	487	23021	N	K	3
C488*	488	23024	C	*	3
S494*	494	23042	S	*	3
S494R	494	23042	S	R	3
S494T	494	23042	S	T	3
G496C	496	23048	G	C	3
Q498*	498	23054	Q	*	3
T500N	500	23060	T	N	3
G502V	502	23066	G	V	3
G504N	504	23072	G	N	3
G504V	504	23072	G	V	3
Y505*	505	23075	Y	*	3
V510A	510	23090	V	A	3
F318C	318	22514	F	C	2
F318I	318	22514	F	I	2
F318V	318	22514	F	V	2
R319K	319	22517	R	K	2
Q321H	321	22523	Q	H	2
Q321R	321	22523	Q	R	2
E324G	324	22532	E	G	2
V327A	327	22541	V	A	2
V327D	327	22541	V	D	2
P330T	330	22550	P	T	2
N331D	331	22553	N	D	2
T333A	333	22559	T	A	2
N334I	334	22562	N	I	2
N334Y	334	22562	N	Y	2

L335S	335	22565	L	S	2
F338V	338	22574	F	V	2
G339R	339	22577	G	R	2
E340V	340	22580	E	V	2
V341F	341	22583	V	F	2
N343D	343	22589	N	D	2
A344P	344	22592	A	P	2
F347C	347	22601	F	C	2
F347Y	347	22601	F	Y	2
A348E	348	22604	A	E	2
A348F	348	22604	A	F	2
A348G	348	22604	A	G	2
V350A	350	22610	V	A	2
V350F	350	22610	V	F	2
Y351C	351	22613	Y	C	2
Y351F	351	22613	Y	F	2
A352T	352	22616	A	T	2
W353S	353	22619	W	S	2
I358F	358	22634	I	F	2
V362I	362	22646	V	I	2
S366F	366	22658	S	F	2
S366L	366	22658	S	L	2
Y369C	369	22667	Y	C	2
Y369D	369	22667	Y	D	2
N370D	370	22670	N	D	2
A372L	372	22676	A	L	2
F374V	374	22682	F	V	2
F377V	377	22691	F	V	2
K378E	378	22694	K	E	2
G381V	381	22703	G	V	2
V382M	382	22706	V	M	2
S383T	383	22709	S	T	2
P384A	384	22712	P	A	2
P384H	384	22712	P	H	2

P384T	384	22712	P	T	2
L387F	387	22721	L	F	2
N388Y	388	22724	N	Y	2
D389G	389	22727	D	G	2
D389H	389	22727	D	H	2
C391F	391	22733	C	F	2
C391S	391	22733	C	S	2
F392I	392	22736	F	I	2
N394K	394	22742	N	K	2
D398V	398	22754	D	V	2
F400S	400	22760	F	S	2
V401A	401	22763	V	A	2
V401I	401	22763	V	I	2
I402F	402	22766	I	F	2
I402T	402	22766	I	T	2
E406G	406	22778	E	G	2
E406K	406	22778	E	K	2
V407F	407	22781	V	F	2
Q409H	409	22787	Q	H	2
Q409K	409	22787	Q	K	2
I410L	410	22790	I	L	2
A411P	411	22793	A	P	2
P412T	412	22796	P	T	2
Q414H	414	22802	Q	H	2
Q414P	414	22802	Q	P	2
K417E	417	22811	K	E	2
I418T	418	22814	I	T	2
A419V	419	22817	A	V	2
N422S	422	22826	N	S	2
Y423H	423	22829	Y	H	2
K424N	424	22832	K	N	2
P426T	426	22838	P	T	2
D428V	428	22844	D	V	2
F429L	429	22847	F	L	2

G431D	431	22853	G	D	2
C432*	432	22856	C	*	2
C432F	432	22856	C	F	2
I434T	434	22862	I	T	2
A435D	435	22865	A	D	2
A435P	435	22865	A	P	2
W436R	436	22868	W	R	2
S438A	438	22874	S	A	2
S438T	438	22874	S	T	2
N439S	439	22877	N	S	2
L441R	441	22883	L	R	2
S443F	443	22889	S	F	2
S443P	443	22889	S	P	2
Y449F	449	22907	Y	F	2
Y449N	449	22907	Y	N	2
Y451*	451	22913	Y	*	2
Y451C	451	22913	Y	C	2
Y451D	451	22913	Y	D	2
L452P	452	22916	L	P	2
Y453*	453	22919	Y	*	2
R454G	454	22922	R	G	2
R454S	454	22922	R	S	2
R454T	454	22922	R	T	2
F456S	456	22928	F	S	2
F456Y	456	22928	F	Y	2
R457W	457	22931	R	W	2
N460H	460	22940	N	H	2
P463T	463	22949	P	T	2
F464I	464	22952	F	I	2
F464V	464	22952	F	V	2
E465V	465	22955	E	V	2
R466G	466	22958	R	G	2
R466I	466	22958	R	I	2
R466S	466	22958	R	S	2

I468L	468	22964	I	L	2
I468N	468	22964	I	N	2
Y473H	473	22979	Y	H	2
Q474K	474	22982	Q	K	2
A475G	475	22985	A	G	2
P479T	479	22997	P	T	2
C480F	480	23000	C	F	2
N487S	487	23021	N	S	2
N487T	487	23021	N	T	2
Y489F	489	23027	Y	F	2
Y489S	489	23027	Y	S	2
F490C	490	23030	F	C	2
P491H	491	23033	P	H	2
L492F	492	23036	L	F	2
Q493P	493	23039	Q	P	2
Y495F	495	23045	Y	F	2
F497L	497	23051	F	L	2
F497S	497	23051	F	S	2
F497V	497	23051	F	V	2
V503L	503	23069	V	L	2
Y505F	505	23075	Y	F	2
Y505N	505	23075	Y	N	2
Q506R	506	23078	Q	R	2
Y508N	508	23084	Y	N	2
R509K	509	23087	R	K	2
R509T	509	23087	R	T	2
F318*	318	22514	F	*	1
F318N	318	22514	F	N	1
R319*	319	22517	R	*	1
R319G	319	22517	R	G	1
V320D	320	22520	V	D	1
P322Q	322	22526	P	Q	1
T323M	323	22529	T	M	1
T323P	323	22529	T	P	1

E324L	324	22532	E	L	1
S325C	325	22535	S	C	1
S325K	325	22535	S	K	1
S325L	325	22535	S	L	1
S325P	325	22535	S	P	1
I326M	326	22538	I	M	1
I326N	326	22538	I	N	1
I326S	326	22538	I	S	1
V327L	327	22541	V	L	1
R328T	328	22544	R	T	1
F329I	329	22547	F	I	1
P330H	330	22550	P	H	1
P330R	330	22550	P	R	1
N331I	331	22553	N	I	1
I332T	332	22556	I	T	1
N334D	334	22562	N	D	1
L335M	335	22565	L	M	1
C336F	336	22568	C	F	1
C336R	336	22568	C	R	1
F338P	338	22574	F	P	1
F338Y	338	22574	F	Y	1
E340Q	340	22580	E	Q	1
V341A	341	22583	V	A	1
V341G	341	22583	V	G	1
V341S	341	22583	V	S	1
F342C	342	22586	F	C	1
N343K	343	22589	N	K	1
N343S	343	22589	N	S	1
T345N	345	22595	T	N	1
T345P	345	22595	T	P	1
F347I	347	22601	F	I	1
F347S	347	22601	F	S	1
F347V	347	22601	F	V	1
A348L	348	22604	A	L	1

A348Q	348	22604	A	Q	1
S349Y	349	22607	S	Y	1
V350Q	350	22610	V	Q	1
Y351N	351	22613	Y	N	1
Y351S	351	22613	Y	S	1
A352G	352	22616	A	G	1
A352P	352	22616	A	P	1
W353*	353	22619	W	*	1
W353F	353	22619	W	F	1
N354Y	354	22622	N	Y	1
R355G	355	22625	R	G	1
R355K	355	22625	R	K	1
R355M	355	22625	R	M	1
K356Y	356	22628	K	Y	1
R357G	357	22631	R	G	1
I358A	358	22634	I	A	1
V362D	362	22646	V	D	1
V362G	362	22646	V	G	1
A363S	363	22649	A	S	1
A363T	363	22649	A	T	1
D364A	364	22652	D	A	1
D364G	364	22652	D	G	1
Y365C	365	22655	Y	C	1
L368R	368	22664	L	R	1
Y369F	369	22667	Y	F	1
A372E	372	22676	A	E	1
S373T	373	22679	S	T	1
F374C	374	22682	F	C	1
S375A	375	22685	S	A	1
S375C	375	22685	S	C	1
T376L	376	22688	T	L	1
F377S	377	22691	F	S	1
C379W	379	22697	C	W	1
Y380*	380	22700	Y	*	1

Y380C	380	22700	Y	C	1
Y380H	380	22700	Y	H	1
G381*	381	22703	G	*	1
G381E	381	22703	G	E	1
G381L	381	22703	G	L	1
V382G	382	22706	V	G	1
S383A	383	22709	S	A	1
T385S	385	22715	T	S	1
K386I	386	22718	K	I	1
L387*	387	22721	L	*	1
N388D	388	22724	N	D	1
N388H	388	22724	N	H	1
N388I	388	22724	N	I	1
N388T	388	22724	N	T	1
D389T	389	22727	D	T	1
L390H	390	22730	L	H	1
L390V	390	22730	L	V	1
C391R	391	22733	C	R	1
F392C	392	22736	F	C	1
F392L	392	22736	F	L	1
F392P	392	22736	F	P	1
T393P	393	22739	T	P	1
Y396D	396	22748	Y	D	1
A397E	397	22751	A	E	1
A397P	397	22751	A	P	1
A397T	397	22751	A	T	1
D398G	398	22754	D	G	1
D398Y	398	22754	D	Y	1
S399A	399	22757	S	A	1
S399T	399	22757	S	T	1
I402S	402	22766	I	S	1
R403*	403	22769	R	*	1
G404A	404	22772	G	A	1
G404D	404	22772	G	D	1

G404R	404	22772	G	R	1
D405H	405	22775	D	H	1
V407D	407	22781	V	D	1
V407R	407	22781	V	R	1
V407S	407	22781	V	S	1
R408*	408	22784	R	*	1
Q409E	409	22787	Q	E	1
Q409L	409	22787	Q	L	1
A411G	411	22793	A	G	1
P412A	412	22796	P	A	1
P412S	412	22796	P	S	1
G413C	413	22799	G	C	1
T415P	415	22805	T	P	1
G416R	416	22808	G	R	1
G416V	416	22808	G	V	1
K417D	417	22811	K	D	1
K417M	417	22811	K	M	1
I418F	418	22814	I	F	1
A419D	419	22817	A	D	1
A419G	419	22817	A	G	1
Y421*	421	22823	Y	*	1
Y421F	421	22823	Y	F	1
Y423*	423	22829	Y	*	1
Y423F	423	22829	Y	F	1
Y423S	423	22829	Y	S	1
K424*	424	22832	K	*	1
K424I	424	22832	K	I	1
K424Q	424	22832	K	Q	1
D427E	427	22841	D	E	1
T430K	430	22850	T	K	1
T430N	430	22850	T	N	1
T430P	430	22850	T	P	1
G431R	431	22853	G	R	1
G431S	431	22853	G	S	1

V433D	433	22859	V	D	1
V433L	433	22859	V	L	1
I434K	434	22862	I	K	1
W436S	436	22868	W	S	1
N437D	437	22871	N	D	1
N437I	437	22871	N	I	1
S438Y	438	22874	S	Y	1
N439*	439	22877	N	*	1
N439D	439	22877	N	D	1
N440H	440	22880	N	H	1
L441V	441	22883	L	V	1
D442A	442	22886	D	A	1
V445D	445	22895	V	D	1
V445G	445	22895	V	G	1
G446R	446	22898	G	R	1
G447A	447	22901	G	A	1
G447R	447	22901	G	R	1
Y449*	449	22907	Y	*	1
N450H	450	22910	N	H	1
N450I	450	22910	N	I	1
L452F	452	22916	L	F	1
Y453S	453	22919	Y	S	1
R454I	454	22922	R	I	1
R454K	454	22922	R	K	1
F456*	456	22928	F	*	1
F456I	456	22928	F	I	1
F456V	456	22928	F	V	1
S459C	459	22937	S	C	1
N460D	460	22940	N	D	1
N460Y	460	22940	N	Y	1
K462*	462	22946	K	*	1
P463A	463	22949	P	A	1
F464C	464	22952	F	C	1
E465K	465	22955	E	K	1

D467G	467	22961	D	G	1
D467H	467	22961	D	H	1
S469P	469	22967	S	P	1
T470S	470	22970	T	S	1
I472F	472	22976	I	F	1
Y473C	473	22979	Y	C	1
Y473D	473	22979	Y	D	1
Q474L	474	22982	Q	L	1
A475D	475	22985	A	D	1
G476F	476	22988	G	F	1
S477C	477	22991	S	C	1
S477D	477	22991	S	D	1
S477K	477	22991	S	K	1
C480G	480	23000	C	G	1
C480S	480	23000	C	S	1
C480W	480	23000	C	W	1
V483D	483	23009	V	D	1
G485D	485	23015	G	D	1
G485T	485	23015	G	T	1
F486I	486	23018	F	I	1
F486V	486	23018	F	V	1
F486Y	486	23018	F	Y	1
N487H	487	23021	N	H	1
C488S	488	23024	C	S	1
C488W	488	23024	C	W	1
C488Y	488	23024	C	Y	1
Y489D	489	23027	Y	D	1
Y489N	489	23027	Y	N	1
F490I	490	23030	F	I	1
F490R	490	23030	F	R	1
P491A	491	23033	P	A	1
P491R	491	23033	P	R	1
P491T	491	23033	P	T	1
L492V	492	23036	L	V	1

Q493E	493	23039	Q	E	1
Y495*	495	23045	Y	*	1
Y495C	495	23045	Y	C	1
Y495N	495	23045	Y	N	1
Y495S	495	23045	Y	S	1
Q498L	498	23054	Q	L	1
Q498P	498	23054	Q	P	1
T500P	500	23060	T	P	1
N501H	501	23063	N	H	1
G502A	502	23066	G	A	1
G502D	502	23066	G	D	1
G502R	502	23066	G	R	1
G502S	502	23066	G	S	1
V503D	503	23069	V	D	1
G504C	504	23072	G	C	1
G504R	504	23072	G	R	1
G504Y	504	23072	G	Y	1
Y505C	505	23075	Y	C	1
Q506H	506	23078	Q	H	1
Q506L	506	23078	Q	L	1
Q506P	506	23078	Q	P	1
P507H	507	23081	P	H	1
Y508F	508	23084	Y	F	1
V510E	510	23090	V	E	1
V510G	510	23090	V	G	1
V510I	510	23090	V	I	1